

1 **Ablation of Amyloid Precursor Protein Increases Insulin Degrading Enzyme Levels and**
2 **Activity in Brain and Peripheral Tissues**

3

4 Joshua A. Kulas¹, Whitney Franklin³, Nicholas A. Smith², Gunjan D. Manocha¹, Kendra L.
5 Puig¹, Kumi Nagamoto-Combs², Rachel D. Hendrix⁴, Giulio Tagliatela⁵, Steven W. Barger^{6,7},
6 Colin K. Combs¹

7 ¹Department of Biomedical Sciences, University of North Dakota School of Medicine and
8 Health Sciences, Grand Forks, ND 58202-9037; ² Department of Pathology, University of North
9 Dakota School of Medicine and Health Sciences, Grand Forks, ND 58202-9037; ³ Department of
10 Neuroscience and Cell Biology, University of Texas Medical Branch, Galveston, TX, USA;
11 ⁴Department of Neurobiology & Developmental Sciences, University of Arkansas for Medical
12 Sciences, Little Rock AR; ⁵Department of Neurology, University of Texas Medical Branch,
13 Galveston, TX, USA. ⁶Department of Geriatrics, University of Arkansas for Medical Sciences,
14 Little Rock AR; ⁷Geriatric Research, Education and Clinical Center, Central Arkansas Veterans
15 Healthcare System, Little Rock AR

16

17 **Running head:** Loss of APP Increases IDE Levels and Activity

18 **Address for Correspondence:** Colin K. Combs, PhD, Department of Biomedical Sciences,
19 Suite W315, 1301 North Columbia Road Stop 9037, University of North Dakota School of
20 Medicine and Health Sciences, Grand Forks, ND 58202-9037. Email:
21 colin.combs@med.und.edu

22

23

24

25 **Abstract**

26 The amyloid precursor protein (APP) is a type-I transmembrane glycoprotein widely studied for
27 its role as the source of β -amyloid peptide, accumulation of which is causal in at least some cases
28 of Alzheimer's disease (AD). APP is expressed ubiquitously and is involved in diverse biological
29 processes. Growing bodies of evidence indicate connections between AD and somatic metabolic
30 disorders related to type-2 diabetes, and *App*^{-/-} mice show alterations in glycemic regulation. We
31 find that *App*^{-/-} have higher levels of insulin-degrading enzyme (IDE) mRNA, protein, and
32 activity compared to wild-type controls. This regulation of IDE by APP was widespread across
33 numerous tissues including liver, skeletal muscle, and brain as well as cell types within neural
34 tissue including neurons, astrocytes, and microglia. RNAi-mediated knockdown of APP in the
35 SIM-A9 microglia cell line elevated IDE levels. Fasting levels of blood insulin were lower in
36 *App*^{-/-} than *App*^{+/+} mice, but the former showed a larger increase in response to glucose. These
37 low basal levels may enhance peripheral insulin sensitivity, as *App*^{-/-} mice failed to develop
38 impairment of glucose tolerance on a high-fat, high-sucrose ("western") diet. Insulin levels and
39 insulin signaling were also lower in *App*^{-/-} brain; synaptosomes prepared from *App*^{-/-}
40 hippocampus showed diminished insulin receptor phosphorylation compared to *App*^{+/+} mice
41 when stimulated *ex vivo*. These findings represent a new molecular link connecting APP to
42 metabolic homeostasis and demonstrate a novel role for APP as an upstream regulator of IDE *in*
43 *vivo*.

44 **Keywords:** Amyloid precursor protein, Insulin degrading enzyme, Alzheimer's disease, insulin,
45 microglia

46

47 **INTRODUCTION**

48 Alzheimer's disease is characterized in part by the robust accumulation of extracellular plaque
49 aggregates of the amyloid β -peptide ($A\beta$) in the central nervous system, and multiple lines of
50 evidence indicates that $A\beta$ is a causal factor in AD (24, 77). While familial AD appears to arise
51 from elevated production of longer (42- or 43-amino acid) forms of $A\beta$, sporadic cases of AD
52 may be more dependent upon compromised clearance of the peptide, which comprises both
53 efflux from the brain into the vasculature and proteolysis. Leading candidates for proteolytic
54 destruction of $A\beta$ include the metalloproteases neprilysin and insulin-degrading peptide (IDE)
55 (5). IDE is a zinc metalloprotease discovered for its ability to hydrolyze insulin, but it has
56 numerous other substrates; in addition to $A\beta$, it is active against pancreatic amylin (44). All
57 insulin-sensitive tissues degrade insulin, and IDE is established to play an important role in
58 regulating insulin signaling and an essential role in insulin catabolism (16).

59

60 $A\beta$ is generated by enzymatic cleavage of the much larger amyloid precursor protein (APP). The
61 genes encoding APP are widely conserved among other species, suggesting the protein performs
62 important or advantageous biological functions (82). APP is part of a three-member family
63 which includes amyloid precursor-like protein (APLP)-1 and -2 (59). While expression of
64 APLP1 is restricted to the central nervous system, both APP and APLP2 are expressed
65 ubiquitously and can be detected in a variety of tissues (49, 78); only APP contains the $A\beta$
66 sequence. APP and APLPs have diverse and critical roles in development and physiology, both
67 in and out of the CNS (8), highlighted by the neonatal lethality of *App/Aplp2* double knockouts
68 (31). Deletion of the *App* gene alone confers a more benign phenotype, including reduced animal

69 body weight and organ size, changes in grip strength and broad changes in metabolism (58, 71,
70 92).

71

72 Mounting evidence indicates connections between AD and perturbations in insulin/glucose
73 regulation related to type-2 diabetes mellitus (T2DM) (28, 33, 51, 57, 80, 81). APP may be
74 involved in these links, as illustrated by several lines of evidence. For instance, genetic ablation
75 of APP perturbs basal glycemic levels (63). A recent report demonstrates numerous metabolic
76 differences in *App*^{-/-} mice, including the finding that circulating levels of insulin are lower in
77 *App*^{-/-} mice (12). In tissue from obese human subjects, increased expression of APP in adipocytes
78 correlates with the degree of insulin resistance, hyperinsulinemia, and plasma A β ₁₋₄₀ levels (47,
79 48). In wild-type C57BL/6 mice, high-fat diet feeding increases the expression of APP in both
80 hippocampus and adipose tissue (72).

81

82 Among its diverse actions, APP contributes to cell adhesion and other aspects of extracellular
83 matrix that appear to involve complex relationships with proteases (85). In addition to its
84 processing by the α -, β -, γ -, and ϵ -secretases, APP itself modulates protease activity. The splice
85 variants expressed in nonneuronal cells contain a Kunitz-type serine protease inhibitor (KPI)
86 domain (9), and other protease inhibitor domains are universal to all splice variants (30, 34). In
87 our recent work, we found that IDE levels are higher in pancreatic tissue extracts and primary
88 pancreatic islet cultures derived from *App*^{-/-} compared to *App*^{+/+} mice (42). In this study we have
89 expanded upon our initial observation of increased IDE in the *App*^{-/-} pancreas by demonstrating
90 that regulation of IDE by APP occurs in other tissues, including the brain, highlighting
91 implications for metabolism of A β .

92

93 **MATERIALS AND METHODS**

94 **Animals**

95 The APP knockout mice (*App*^{-/-}) strain B6.129S7-*App*^{tm1Dbo}/J ([https://www.jax.org/](https://www.jax.org/strain/004133)
96 strain/004133) and wild-type (*App*^{+/+}) C57BL/6 mice, were purchased from the Jackson
97 Laboratory (Bar Harbor ME). APP is knocked out in *App*^{-/-} mice by deletion of the promoter
98 region and Exon 1 of the *App* gene (92). Both male and female mice were utilized in this study.
99 Where indicated, normal mouse chow was replaced with “western diet” (ENVIGO TD.88137):
100 42% kcal from fat, 34% sucrose by weight. Western diet TD.88137 has the following
101 composition by weight: 17.3% protein, 48.5% carbohydrates and 21.2% fat with a calorie
102 content of 4.5 kcal/g. Two control diets were used (ENVIGO TD.08485 and LabDiet JL Rat and
103 Mouse/Auto 6F FK67) having 17 – 19% protein, 55 – 61% carbohydrate, and 5.2 – 7.3% fat by
104 weight. Control diets had a composition of 13 – 16% kcal from fat and 3.45 – 3.60 kcal/g. Such
105 studies began with experimentally naïve male mice that were 8 weeks of age (first GTT), and
106 diets deviated at 9 weeks of age. Animals were euthanized by CO₂ asphyxiation and cardiac
107 exsanguination and blood was cleared by perfusion with phosphate-buffered saline. Animal use
108 was approved by the University of North Dakota Institutional Animal Care and Use Committee
109 and the Central Arkansas Veterans Healthcare System Animal Care and Use Committee. Mice
110 were provided with food and water *ad libitum* and housed in a 12-hour light/dark cycle. This
111 study conforms to the National Research council of the National Academies Guide for the Care
112 and Use of Laboratory Animals.

113

114 **Antibodies**

115 Antibodies against full-length APP (ab32136), IDE (ab32216) were purchased from Abcam
116 (Cambridge, MA) (10, 43). Antibodies p-AKT Thr308 (13038) and AKT (C67E7) were
117 purchased from Cell Signaling Technology, Inc. (Danvers MA). The polyclonal antibody against
118 IDE utilized for immunohistochemistry was purchased from Biogen product 840301 (San
119 Diego CA) and was formerly available from Covance as product PRB-282C (88). Anti-GAPDH
120 antibody (6C5) and HRP-conjugated secondary antibodies were purchased from Santa Cruz
121 Technologies (Santa Cruz CA). Antibodies used in WES capillary western blots included β -
122 tubulin (Cell Signaling #2146S), insulin receptor (Cell Signaling #3025S), and p-IGF1R-IR β
123 (Cell Signaling #3024S).

124

125 **RNA Extraction and RT-qPCR**

126 Total RNA from hippocampus tissue from *App*^{+/+} and *App*^{-/-} mice was isolated using Trizol
127 Reagent (Thermo Fisher Scientific, Waltham MA) according to the manufacturer's instruction.
128 Briefly, the tissue samples preserved in Allprotect Tissue Reagent (Qiagen Inc., Valencia CA)
129 were washed once with PBS and homogenized in Trizol using a Bullet Blender Storm 24 tissue
130 homogenizer (Next Advance, Inc., Averill Park NY) with 5-mm stainless-steel beads (Qiagen).
131 Extracted RNA samples were quantified using a NanoDrop spectrophotometer (Thermo Fisher
132 Scientific). For each sample, cDNA was generated from 1 μ g of total RNA using iScript
133 Reverse Transcription Supermix (Bio-Rad Laboratories, Hercules CA) per the manufacturer
134 specifications. A previously described primer set for *Ide* (forward: 5'-
135 CTGTGCCCTTGTTTGATGC-3'; reverse: 5'-GTTCCCCGTAGCCTTTTCCA-3') (43) was
136 purchased from Millipore Sigma (St. Louis MO). qPCR was performed in triplicates using iTaq
137 Universal SYBR Green Supermix and CFX96 Touch™ Real-Time PCR Detection System with

138 CFX Manager 3.0 software (Bio-Rad). Ribosomal protein 18S (PrimePCR SYBR Green Assay
139 Rsp18, Bio-Rad) was used as a reference gene and *Rsp18* Cq values were used to normalize
140 respective *Ide* Cq values (Δ Cq). Relative *Ide* mRNA expression was determined as $2^{-\Delta\Delta Cq}$ and
141 shown as mean \pm SEM for each mouse strain.

142

143 **Cell lines and cell culture**

144 **Microglia cell line.** The SIM-A9 mouse microglial cell line was previously developed and
145 characterized in our laboratory (60) and is available from ATCC (ATCC CRL-3265). The cells
146 were grown in DMEM/F12 (ThermoFisher Scientific product 12400024) supplemented with
147 10% FBS and penicillin, neomycin, and streptomycin.

148 **Mouse Neuron Primary Culture.** Neurons were cultured from *App*^{+/+} and *App*^{-/-} brains on
149 embryonic day 16 (4, 19, 36, 67). Embryos were harvested and brains were placed into sterile
150 dissection media (0.5 mM EDTA, 100 μ M EGTA, 5.5 mM glucose, in PBS). Meninges were
151 removed, and cortices were harvested from both hemispheres, minced in dissection media, and
152 treated with 0.25% trypsin. Tissue was digested for 20 min at 37 °C. Digestion was terminated
153 by adding 10 ml DMEM/F12 containing 10% FBS. The cells were then allowed to settle in the
154 bottom of the pipette tip and then added to 10 ml of Neurobasal media supplemented with B27
155 and L-Glutamine, penicillin, streptomycin and neomycin, then triturated approximately 20 times.
156 Cells were cultured in 6-well plates coated overnight with poly-L-lysine. Neuron cultures were
157 grown at 37 °C in 5% CO₂ (54).

158 **Mouse Primary Microglia and Astrocyte Culture.** Microglia and astrocyte cultures were
159 established from 1-day-old *App*^{+/+} and *App*^{-/-} neonatal pups as previously described (54).

160 Meninges were removed from cerebrum, and cortical tissue was harvested in dissection media

161 (0.5 mM EDTA, 100 μ M EGTA, 5.5 mM glucose, in PBS) on ice. Cortices were then digested in
162 trypsin for 15 min at 37 °C. Digestion was terminated using DMEM/F12 media containing 10%
163 FBS. Cortical tissue from each mouse was cultured separately in a T75 flask with 20 ml of
164 DMEM/F12 supplemented with 10% FBS, penicillin, streptomycin and neomycin. Media was
165 supplemented on Day 2 and replaced after one week. After two weeks of culture, microglia were
166 separated from astrocytes by shaking flasks at 200 RPM for 45-60 min. The microglial
167 suspension was collected and plated for microglial culture. Astrocytes adherent to the flasks were
168 removed with trypsin and cultured on 6-well plates for experiments.

169

170 **Glucose tolerance test (GTT) and Insulin tolerance test (ITT)**

171 Beginning at 7 weeks of age, blood was collected from male mice and blood glucose ($[Glc]_b$)
172 was measured using a glucometer (AlphaTRAK II, Abbott Laboratories). For GTT, mice were
173 fasted 4 h (with access to water); $[Glc]_b$ was determined prior to intraperitoneal injection of Glc
174 (2 mg/g) and at 15, 30, 60, 120 min thereafter. Some GTT results are expressed as incremental
175 area under the curve (AUC); the difference between initial $[Glc]_b$ and subsequent $[Glc]_b$ values
176 ($T_N - T_0$) for each mouse was used for this calculation to remove differences in basal $[Glc]_b$. For
177 ITTs, $[Glc]_b$ was determined in non-fasted mice prior to i.p. injection of insulin (0.75 U/g) and at
178 15, 30, 60, and 120 min thereafter. GTT and ITT were performed on the same day of the week
179 in alternating weeks. Some ITT results are expressed as incremental area over the curve (AOC);
180 the difference between initial $[Glc]_b$ and subsequent $[Glc]_b$ values ($T_0 - T_N$) for each mouse was
181 used for this calculation to remove differences in basal $[Glc]_b$. For experiments in aged animals,
182 mice were fasted 5 h (with access to water); $[Glc]_b$ was determined prior to intraperitoneal
183 injection of Glc (2 mg/g) and at 15, 30, 60, 120 min thereafter.

184

185 **Insulin ELISA**

186 Blood (25-30 μ l) was collected at the 0- and 30-min time points during the GTT performed at
187 Week 6 of the western-diet feeding and centrifuged for 10 min at 2000 *g* and 4° C to extract
188 serum. Insulin concentrations were measured from 10- μ l aliquots of serum using an Ultra-
189 Sensitive Mouse Insulin ELISA Kit (Crystal Chem Inc.) according to manufacturer's protocol.

190

191 **RNAi knockdown of APP**

192 RNAi-mediated knockdown of the mouse APP gene in SIMA9 microglia was achieved using
193 Dharmacon (Lafayette CO) Accell SMARTpool siRNA (product E-043246-00-0050), with non-
194 targeting RNA (product D-001910-01-50) treated cells used as controls. The siRNA was utilized
195 by combining the Accell siRNA with Accell delivery media per manufacturer's instructions, and
196 cells were treated with 1 μ M RNA for 6 days. After 3 days of treatment (72 h), siRNA
197 containing media was supplemented 1:1 with normal DMEM/F12 with 10% FBS. SIMA9 cell
198 protein was harvested on Day 7 for western blot analyses.

199

200 **Western blot analyses**

201 Hippocampus, gastrocnemius, liver tissues and primary cell cultures were lysed in
202 radioimmunoprecipitation assay (RIPA) buffer containing protease inhibitor (Sigma P8340, St.
203 Louis MO) on ice. Protein concentrations were determined using the Bradford method (3). Five
204 to ten μ g of protein was resolved by 10% SDS-PAGE and transferred to PVDF membranes.
205 Membranes were blocked for 1 h in Tris-buffered saline containing Tween-20 (TBST) and 5%
206 BSA solution, and then they were incubated overnight in 5% BSA-TBST solution containing the

207 primary antibody. The next day primary antibodies were washed off the membrane with TBST,
208 and HRP-conjugated secondary antibodies were applied to membranes in 5% BSA-TBST for 2
209 h. Luminol chemiluminescence was utilized for visualization of proteins with and Aplegen
210 Omega Lum G Gel Documentation System (Gel Company, San Francisco, CA). Western blot
211 analysis was performed using Adobe Photoshop CS6 (Adobe Systems, San Jose, CA). To
212 quantify western blot bands (ie IDE), a box was traced around the protein band of interest. The
213 mean pixel intensity of the area of the box was then measured using the histogram. The box was
214 then moved to additional bands until all bands of interest were quantified. The measured values
215 of bands of interest were then normalized to the mean intensity of the loading control protein for
216 each individual sample. Finally, all normalized protein values were divided by the mean of the
217 *App*^{+/+} condition to obtain a mean of 1.0 for *App*^{+/+} samples.

218

219

220 **IDE Activity Assays**

221 The IDE activity assays were purchased from AnaSpec (Fremont, CA) (Catalog # AS-72231).
222 The assay utilizes a FRET substrate which emits increased fluorescence when cleaved by IDE.
223 This increased fluorescence is due to liberation of 5-carboxyfluorescein (5-FAM) from a
224 quenching molecule also on the IDE substrate. Hippocampus, liver, and gastrocnemius were
225 collected on ice from *App*^{+/+} and *App*^{-/-} mice. Our preliminary experiments utilizing this assay
226 suggested that IDE enzyme activity is negatively affected by sonication. Tissue was
227 homogenized on ice in assay buffer using a Powermasher II (Nippi, Japan). Fifty μ l of individual
228 brain homogenate was loaded into a well of a 96-well plate containing 50 μ l of substrate
229 solution. The fluorescence intensity was measured on a Biotek Plate reader using an excitation of

230 485 nm and emission of 528 nm at 5-min increments. Fluorescent units measured were converted
231 to concentrations of 5-FAM. The protein concentration of each tissue homogenate was
232 determined using the Bradford method and 5-FAM concentrations were normalized to the total
233 protein in each sample. Total IDE activity in each sample was calculated using the formula
234 $([\text{Final Concentration}] - [\text{Initial Concentration}] / \text{Time} \times \text{Volume}) \times \text{Dilution Factor}$ described by
235 Kurauti et al. and normalized as described above (43).

236

237 **Immunohistochemistry**

238 Left hemispheres of mouse brains were fixed in 4% paraformaldehyde/PBS for 48 h and
239 embedded in a 15% gelatin matrix as described previously (61). The brains were cryosectioned
240 into 40- μm serial sections by a sliding microtome (Leica SM 2000R, Leica Biosystems Inc.,
241 Buffalo Grove, IL). The free-floating sections were incubated in the anti-IDE antibody diluted
242 1:200 overnight at 4 °C in PBS containing 1% Triton X-100, 3% BSA, 2% horse serum.
243 Visualization of the antigen was carried out using a VECTASTAIN Elite ABC-HRP Kit with
244 VIP as the chromogen (Vector Laboratories, Burlingame, CA). The brain sections were mounted
245 onto subbed glass slides and dehydrated through an ethanol gradient prior to coverslipping using
246 Permount mounting medium (ThermoFisher).

247

248 **APP Plasmids and Transfections**

249 pCAX APP 751 and pCAX APP 695 were a gift from Drs. Dennis Selkoe & Tracy Young-
250 Pearse and are available from Addgene as plasmids 30138 and 30137 (89). Plasmids were
251 prepared using Qiagen Endofree Plasmid Giga Kit (product 12391). Primary astrocyte cultures

252 were transfected using Lipofectamine 3000 (ThermoFisher Scientific) as per the manufacturer
253 instructions.

254

255 **APP peptides**

256 Bacterial recombinant sAPP α 695 was purchased from Sigma Aldrich (Product number S9564).

257 Other sAPP peptides utilized in this study were expressed in an eukaryotic system. HEK293 cells

258 stably transfected with a vector encoding human APP751₁₋₆₆₈, APP695₁₋₆₁₂, were grown to

259 subconfluency in T175 flasks and changed to a serum-free medium supplemented with 0.5 mM

260 L-glutamine, 50 μ M ethanolamine, and 10 nM sodium selenite. After four days, the conditioned

261 medium was loaded onto a 15-ml DE52 column to concentrate the acidic proteins. The column

262 was eluted with phosphate buffer (pH 7.4) containing 0.75 M NaCl, 0.5 mM

263 ethylenediaminetetraacetic acid (EDTA), and 1 mM phenylmethylsulfonyl fluoride (PMSF); 1-

264 ml fractions were collected. The fractions containing sAPP α (determined by immunodetection

265 on dot blots) were pooled, dialyzed 1 h at 4 °C versus 2 L of PBS (pH 7.4) containing 1 mM

266 EDTA, 1 mM PMSF; the dialysate was loaded onto a 5-ml Supelco Hi-Trap heparin column (GE

267 Healthcare). The heparin column was eluted with an FPLC pump-controlled salt gradient,

268 starting with 20 mM phosphate buffer (pH 7.4) containing 150 mM NaCl, 1 mM EDTA, and 1

269 mM PMSF and finishing with the same buffer containing 1 M NaCl; 0.5-ml fractions were

270 collected. The sAPP α -containing fractions were pooled, dialyzed 1 h at 4 °C versus 2 L of 20

271 mM Tris-HCl, pH 8, containing 20 mM NaCl, 1 mM EDTA, and 1 mM PMSF; the dialysate was

272 loaded onto a Bio-Scale Q5 anion-exchange column (Bio-Rad). The Q5 column was eluted with

273 an FPLC pump-controlled salt gradient, starting with a 20 mM Tris-HCl buffer (pH 8) containing

274 20 mM NaCl, 1 mM EDTA, and 1 mM PMSF and finishing with the same buffer containing 1 M

275 NaCl; 0.5-ml fractions were collected. The sAPP α -containing fractions were further analyzed by
276 SDS-PAGE with silver staining.

277
278 Recombinant bacterial-produced APP fragments were applied at a concentration of 20 nM in
279 serum-free DMEM/F12, while eukaryotic produced fragments were applied at a concentration of
280 200 nM. Fragments were applied for a total of 72 h and refreshed at 24 and 48 h.

281

282 **Secretase inhibitor treatment**

283 Secretase inhibitors were applied to SIMA9 cells in DMEM/F12 supplemented with 1% FBS,
284 penicillin, streptomycin, and neomycin for one week at a concentration of 1 μ M. Fresh inhibitors
285 and media were applied daily to the cells. Neither overt toxicity nor increased LDH activity in
286 cell culture media was observed. LDH activity assays were purchased from Cayman Chemical
287 (Product number 601170) and were performed per manufacturer's instructions. The α -secretase
288 inhibitor, GI254023X, was purchased from Sigma Aldrich. The recently described β -secretase
289 inhibitor, Verubescestat, was purchased from Selleckchem (Houston TX). The widely used γ -
290 secretase inhibitor, DAPT, was purchased from Sigma Aldrich. The dose of 1 μ M is well above
291 the IC₅₀ value of Verubescestat, reported at 3.4 nM for murine BACE1. The reported IC₅₀ for
292 DAPT is 0.02 μ M. The reported IC₅₀ for GI254023X inhibition of ADAM10 is 5.3 nM (15, 32,
293 38, 50).

294

295 **Hippocampus synaptosome preparation and stimulation**

296 Synaptosomal insulin responsiveness was evaluated by *ex vivo* stimulation of isolated
297 synaptosomal preparations as previously described (21). Briefly, frozen *App*^{+/+} and *App*^{-/-} mouse

328 hippocampi were homogenized using SynPER reagent (Thermo Scientific) with 1 % protease
329 inhibitor cocktail and phosphatase inhibitor cocktail, and homogenates were centrifuged at 1230
330 g for 10 min at 4 °C. The supernatant was collected and centrifuged once more at 15,000 g for 20
331 min at 4 °C. The pellet was resuspended in a physiological buffer, HEPES-buffered Krebs-like
332 (HBK) buffer (143 mM NaCl, 4.7 mM KCl, 1.3 mM MgSO₄, 1.2 mM CaCl₂, 20 mM HEPES,
333 0.1 mM NaH₂PO₄, and 10 mM D-glucose, pH 7.4), and aliquoted into tubes of equal protein for
334 unstimulated and insulin-stimulated samples. All tubes received 8 mM ATP, and insulin
335 stimulation was performed with 10 nM or 200 nM of diluted U-100 insulin. All tubes were
336 incubated at 37 °C for 15 min. Samples were pelleted at 10000 g for 10 min at 4 °C and
337 resuspended in RIPA buffer (75 mM NaCl, 25 mM Na₂PO₄, 1 mM EDTA, 0.5% NP-40, and
338 0.5% TritonX-100) plus 1% protease inhibitor cocktail and phosphatase inhibitor cocktail. The
339 bicinchoninic acid assay method was used to prepare samples of equal protein concentration for
340 WES capillary western blot technology (ProteinSimple, San Jose CA). Data is reported as area
341 under the peak for the specified proteins.

342

343 **Statistical Analysis**

344 Statistical analysis was performed using SigmaPlot 12.0 software. Values were averaged ± SEM
345 and statistical significance was determined via Student's t-test or one-way ANOVA as
346 appropriate. In the case of statistical significance, the Tukey-Kramer *post hoc* test or Holm-Sidak
347 multiple pair-wise comparisons were used where applicable. The difference in the mean relative
348 *Ide* mRNA expression values was statistically analyzed by performing unpaired t-test with
349 Welch correction factor using GraphPad Prism 7.03 software (GraphPad Software, Inc., La Jolla,
350 CA). P-values less than 0.05 were considered statistically significant.

321

322 RESULTS

323

324 IDE protein and mRNA were increased in *App*^{-/-} tissues

325

326 We began examining the potential role of APP in regulating IDE in skeletal muscle from two-
327 month-old female *App*^{+/+} C57BL/6 and *App*^{-/-} mice via western blot analysis of homogenates. As
328 expected, APP was not detectable in gastrocnemius tissue collected from *App*^{-/-} mice but was
329 detectable in *App*^{+/+} controls (Figure 1A). Interestingly, IDE protein levels were found to be
330 significantly higher in *App*^{-/-} muscle (n=6, P<0.001) compared to the controls. Next, we
331 examined liver tissue collected from *App*^{+/+} and *App*^{-/-} animals (Figure 1B). Similar to the
332 skeletal muscle, we observed higher IDE protein levels in liver tissue extracts from *App*^{-/-} mice
333 compared to *App*^{+/+} controls (n=7, p=0.023). These data, along with our previous observations of
334 elevated IDE protein in pancreatic extracts from *App*^{-/-} mice (42), suggested that APP negatively
335 regulates IDE levels in numerous peripheral tissues.

336

337 Due to the potential role of IDE in A β clearance, we next sought to examine if ablation of the
338 APP gene altered IDE protein levels in the brain. To identify which cell types may be most
339 abundantly expressing IDE, we performed immunohistochemistry to detect IDE in *App*^{+/+} and
340 *App*^{-/-} brain tissue. IDE was diffusely detectable throughout the brain, including within the white
341 matter. Although neurons within the hippocampus were stained to a greater extent, IDE
342 immunostaining did not specifically label a single cell type in the CNS. This is in agreement with
343 previous research demonstrating the expression of IDE in multiple cell types of the brain

344 including neurons, astrocytes and microglia (see <http://www.brainrnaseq.org/>) (91). Because of
345 this high expression, as well as the critical roles in normal memory and AD pathology played by
346 the hippocampus, we assessed IDE protein levels in this region from *App*^{+/+} and *App*^{-/-} brains by
347 western blot (n=6-7) (Figure 1C). IDE protein levels were found to be almost three-fold higher
348 in *App*^{-/-} hippocampus tissues compared to *App*^{+/+} controls (p<0.001). This suggested that APP
349 regulation of IDE extends to the central nervous system and is not limited to peripheral organs.
350 We then examined mRNA levels to examine whether APP may be regulating IDE at the
351 transcriptional or post-translational levels. When relative abundance of *Ide* transcripts were
352 determined using RT-qPCR (n=4/5), we observed a significantly higher level of *Ide* mRNA in
353 *App*^{-/-} hippocampus tissue compared to *App*^{+/+} controls (p=0.002) (Figure 1D). Similar to protein
354 levels of IDE, we observed a difference in *Ide* mRNA expression in *App*^{-/-} hippocampus tissue of
355 greater than three-fold compared to *App*^{+/+} controls. Collectively, these data suggested that APP
356 acts as a negative regulator of IDE levels and that ablation of APP increases IDE at the levels of
357 transcription and protein. Furthermore, our immunohistochemistry suggests that IDE is produced
358 throughout the brain in many cell types, and IDE expression is particularly increased in
359 hippocampal neurons in *App*^{-/-} mouse brain.

360

361 **IDE expression was dependent on APP levels in cultured neurons, astrocytes and microglial** 362 **cells**

363

364 Following our observation that mRNA and protein levels for IDE were robustly increased in the
365 hippocampus tissue of *App*^{-/-} mice, we next sought to determine which cell type(s) found in the
366 brain are responsible for the difference in IDE content. (Figure 2A). As expected, APP was

367 abundant in *App*^{+/+} cultures of cortical neurons and not detectable in *App*^{-/-} cultures. Consistent
368 with our observations in homogenized hippocampus, total IDE protein levels were significantly
369 higher in *App*^{-/-} neuronal cultures compared to *App*^{+/+} controls (n=4, p<0.010). We also
370 established cultures of astrocytes and microglia from *App*^{+/+} and *App*^{-/-} mice to determine if APP
371 regulates IDE protein in these glial cell types in a manner similar to neurons (n=3/condition).
372 The APP detected in cultures of astrocytes and microglia had lower mobility, predicted from the
373 differential expression of KPI-containing splice variants in these various cell types. IDE protein
374 levels were found to be significantly higher in both astrocyte (Figure 2B; p=0.009) and microglia
375 (Figure 2C, p=0.009) cultures relative to *App*^{+/+} controls. These data suggested that APP
376 regulates IDE in both neurons and glia and is not restricted to a specific isoform of APP
377 expressed in limited cell types. Furthermore, this suggests that multiple cell types are responsible
378 for increased total IDE levels found in *App*^{-/-} hippocampus extracts.

379

380 Given that we observed increased IDE in *App*^{-/-} microglia and that microglial IDE may be
381 particularly important for degrading A β , we next tested the hypothesis that knockdown of APP
382 with siRNA in the SIMA9 microglial cell line will increase IDE levels *in vitro* (Figure 2D).
383 Knockdown of APP protein was performed over 1 week with either an anti-*App* siRNA pool or a
384 scrambled RNA control (n=6/condition). As expected, treatment with anti-*App* siRNA
385 significantly reduced APP as measured by western blot (p=0.003). IDE protein levels were
386 robustly and significantly increased in microglia (p<0.001) treated with anti-*App* siRNA,
387 suggesting that knockdown of APP *in vitro* is sufficient to increase IDE protein levels in cultured
388 cells. This also suggests that APP has a direct role in regulating IDE and that the increased levels

389 of IDE observed in the *App*^{-/-} mice is not a consequence of overall differences in the physiology
390 of the animals.

391

392 **IDE activity was increased in *App*^{-/-} tissues**

393

394 To confirm a potential impact on substrates of the differential levels of IDE protein, we also
395 compared the enzymatic activity of IDE in *App*^{+/+} and *App*^{-/-} mouse tissues. To measure IDE
396 activity we utilized a commercially available IDE activity assay. This assay uses a FRET peptide
397 IDE substrate that emits increased 5-FAM fluorescence when hydrolyzed by the IDE enzyme.
398 Hippocampus, gastrocnemius, and liver tissue was collected from 2-month-old *App*^{+/+} and *App*^{-/-}
399 mice (n=6 per condition) and homogenized. Each tissue homogenate was then mixed with the
400 IDE substrate, and fluorescence was measured over time (Figure 3). The IDE activity of each
401 tissue extract was calculated and normalized to the total protein content of the sample.

402 Significantly higher IDE activity was observed in *App*^{-/-} hippocampus (p=0.016) and liver
403 extracts (p=0.003), indicating that the higher IDE protein likely leads to differences in the
404 stability of IDE substrates in these tissues. Unlike hippocampus and liver tissue, no significant
405 differences in IDE activity were observed between *App*^{+/+} and *App*^{-/-} gastrocnemius tissue
406 extracts (p=0.746).

407

408 **Insulin levels and insulin signaling were altered in *App*^{-/-} hippocampus tissue and** 409 **synaptosomes**

410

411 We next sought to probe for consequences of increased IDE protein and enzyme activity on
412 insulin levels and insulin signaling markers in hippocampus tissue. We measured the insulin
413 levels of 2-month-old *App*^{+/+} and *App*^{-/-} hippocampus extracts by ELISA (n=11/13).
414 Hippocampus extracts from *App*^{-/-} mice had significantly lower hippocampal insulin levels
415 compared to *App*^{+/+} animals (p=0.032), suggesting that total insulin levels in the brain is reduced
416 in these animals (Figure 4A). We next examined hippocampus extracts from *App*^{+/+} and *App*^{-/-}
417 mice for changes in insulin signaling markers. While we were unable to clearly detect
418 phosphorylated insulin receptor in these lysates (Figure 4B), we also examined the T308 residue
419 of AKT, as it is well-established to be phosphorylated in response to insulin signaling (1). We
420 observed significantly lower (p=0.025) levels of pAKT T308 in *App*^{-/-} hippocampal lysates
421 compared to *App*^{+/+} controls, suggesting that *App*^{-/-} animals have diminished insulin signaling in
422 brain tissue.

423

424 To further examine insulin signaling in the brains of these animals, we prepared synaptosomes
425 from *App*^{+/+} and *App*^{-/-} brain tissues and stimulated them acutely with insulin *ex vivo*. Stimulated
426 synaptosome lysates were then analyzed for protein and phosphorylated protein content by the
427 WES capillary western blot. We have previously utilized this method to examine insulin
428 signaling in the brains of other transgenic mice (73), and the details of this method have been
429 expanded upon in recent literature (21). *App*^{+/+} and *App*^{-/-} synaptosomes were stimulated with
430 either 10 or 200 nM insulin (n=4-6/condition). Interestingly, *App*^{-/-} synaptosomes showed
431 diminished phosphorylation of the insulin receptor compared to *App*^{+/+} synaptosomes when
432 stimulated with either 10 nM (p=0.0315) or 200 nM (p=0.0265) insulin. (Figure 4C). No
433 differences in the ratio of phosphorylated insulin receptor (IR) to total insulin receptor were

434 observed in the unstimulated synaptosomes. These data suggest that *App*^{-/-} animals have impaired
435 insulin signaling in the brain at the level of the insulin receptor.

436

437 ***App*^{-/-} mice had low basal levels of circulating insulin and were protected from impairment**
438 **of glucose tolerance by western diet**

439

440 While our data suggest *App*^{-/-} animals have changes in brain insulin signaling, their higher levels
441 of IDE in peripheral tissues suggested they might exhibit somatic effects as well. Paradigms of
442 diet-induced obesity have been documented to elevate markers of metabolic syndrome, such as
443 impaired glucose tolerance secondary to insulin resistance. We fed *App*^{+/+} and *App*^{-/-} littermates a
444 “western” diet (WD, high fat and high sucrose) for 13 weeks. Consistent with previous studies,
445 *App*^{+/+} mice on the WD showed impaired glucose tolerance in glucose tolerance tests (GTT). At
446 Week 0 (7 weeks of age), prior to the introduction of WD, *App*^{+/+} and *App*^{-/-} showed nearly
447 identical responses to glucose challenge (not shown). By Week 8 (7 weeks of diet manipulation;
448 15 weeks of age), *App*^{+/+} mice showed blood glucose concentrations ([Glc]_b) that were higher on
449 WD compared to normal diet (ND) controls (Fig. 5A). Conversely, the [Glc]_b in *App*^{-/-} mice fed
450 WD was not different from ND controls. To ascertain that the differences in GTT involved
451 differences in glucose excursion, independent of differences in initial [Glc]_b, the GTT profiles
452 were integrated as area under the curve (AUC) using at each time point [Glc]_b values from which
453 the initial [Glc]_b had been subtracted individually for each animal. The mean of these values
454 over weeks 14 – 20 (13 – 19 weeks on diet) showed an overall impairment of glucose tolerance
455 in *App*^{+/+} mice fed WD, but *App*^{-/-} mice failed to reach this state on either diet (Fig. 5B). In
456 addition, WD raised fasting [Glc]_b in *App*^{+/+} but not *App*^{-/-} mice.

457
458 An insulin tolerance test (ITT) was used to evaluate insulin sensitivity on weeks alternating with
459 the GTT. At Week 1 (7 weeks of age; prior to dietary manipulation) *App*^{+/+} and *App*^{-/-} mice had
460 similar insulin sensitivity, with *App*^{-/-} mice trending toward a more robust response (data not
461 shown). By Week 9 (16 weeks of age; 8 weeks on WD), there was a significant difference in the
462 WD-fed mice as a function of genotype (Fig. 5C). To ascertain that the difference between
463 *App*^{+/+} and *App*^{-/-} mice reflected differences in insulin resistance and was independent of
464 differences in initial [Glc]_b, the area of the deflection from the initial [Glc]_b over time was
465 integrated. In contrast to the GTT calculations, ITTs were integrated as area over the curve
466 (AOC): For this calculation, the [Glc]_b at each time point was subtracted from the initial [Glc]_b,
467 in effect setting the ceiling for the curve at the initial [Glc]_b for each animal. The mean of these
468 values over weeks 13 – 19 (12 – 18 weeks on diet) showed insulin resistance in *App*^{+/+} mice fed
469 WD, but *App*^{-/-} mice were protected from this outcome (Fig. 5D).

470
471 The above results indicate that *App*^{-/-} mice retained greater insulin sensitivity than their *App*^{+/+}
472 counterparts on a WD. We measured blood insulin levels in a fasted state and 30 min after a
473 glucose injection. While the *App*^{+/+} mice fed WD clearly exhibited hyperinsulinemia, *App*^{-/-} mice
474 maintained normal basal insulin levels on this diet (Table 1). In fact, *App*^{-/-} mice on normal and
475 western diet had lower fasting insulin levels than their *App*^{+/+} counterparts, potentially
476 implicating a role for elevated IDE in regulating circulating insulin levels. Due to the low basal
477 levels of insulin observed in the fasting state of *App*^{-/-} mice, the change in insulin levels in
478 response to glucose was much greater in these animals.

479

480 **Aged *App*^{-/-} mice have normal glucose tolerance but are hypoglycemic when fasted**

481 Aging is a well-established risk factor for both diabetes and Alzheimer's disease (37, 66). While,
482 as stated above, we found no differences in glucose tolerance in young *App*^{-/-} animals on a
483 normal chow diet compared to *App*^{+/+} controls, we also tested 12-month old cohorts of both
484 *App*^{+/+} and *App*^{-/-} mice (n=11/13) on normal chow to examine the potential consequences that
485 may result from the increased levels of IDE while aging (Figure 6). Animals were fasted for 5
486 hours on the day of the experiment and then administered 2g/kg body weight glucose by
487 intraperitoneal injection. Blood glucose was monitored just prior to injection and at 15, 30, 60
488 and 120 minutes after injection. Data was graphed as blood glucose versus time and the area
489 under the curve was assessed. No significant difference was observed in overall glucose
490 tolerance (p=0.12) between *App*^{+/+} and *App*^{-/-} mice. However, we did observe a robust and
491 significant reduction in the fasting blood glucose levels of *App*^{-/-} mice (p=0.002) compared to
492 *App*^{+/+} controls. Blood glucose was also measured in free-fed *App*^{+/+} and *App*^{-/-} mice
493 (n=5/condition) and was not significantly different (p=0.221). These data suggest aged *App*^{-/-}
494 mice on normal chow remain glucose tolerant but are hypoglycemic when fasted, potentially
495 indicating that increased IDE levels at older ages may have consequences on normal glucose
496 homeostasis.

497

498 **Overexpression of APP or treatment with secretase inhibitors did not alter IDE levels**

499

500 APP is cleaved by a variety of enzymes termed secretases, which result in the production of
501 various APP fragments. To examine if IDE regulation occurs in an APP fragment-specific
502 manner and if selective inhibition of secretase isotypes differentially alter levels of IDE, SIM-A9

503 microglia cells were treated for 7 days in DMEM with 1% serum in the presence or absence of
504 GI254023X (α -secretase inhibitor), Verubecestat (β -secretase inhibitor), or DAPT (the γ -
505 secretase inhibitor) (Fig. 7A). SIM-A9 cells were chosen for this experiment as they are
506 amenable to culturing in low-serum conditions and had shown an increase in IDE protein levels
507 when APP was knocked down with siRNA (Figure 2D). No overt toxicity or change in LDH
508 activity in the media was observed from this treatment (data not shown), indicating the secretase
509 inhibitors did not cause robust cell death. No significant difference was found in the IDE protein
510 content of SIM-A9 cells treated with inhibitors compared to untreated or vehicle controls
511 (n=3/treatment, p=0.45) (Figure 7A).

512

513 Next, to further examine if a specific APP metabolite may be capable of changing IDE levels, we
514 tested if recombinant sAPP fragments would reduce protein levels of IDE in *App*^{-/-} astrocyte
515 primary cultures. sAPP is thought to exert effects on cells by inducing signaling through a
516 variety of receptors (26). Cells were treated for 3 days with 20 nM of prokaryotically expressed
517 recombinant sAPP α , sAPP β , or mutant sAPP α lacking N-terminal amino acids 304-612;
518 eukaryotically expressed sAPP α 695 or sAPP α 751 were also tested at 200 nM. These sAPP
519 fragments did not alter IDE levels in cultures, indicating that the full-length APP protein or
520 another APP fragment is required for differences in IDE levels observed in *App*^{-/-} tissues (Fig.
521 7B).

522

523 Finally, we tested if overexpression of the APP695 isoform or the APP751 isoform in *App*^{-/-}
524 astrocytes was sufficient to reduce levels of IDE. Primary astrocyte cultures were either mock
525 transfected or transfected with plasmids coding for APP695, APP751 or green fluorescent

526 protein (GFP). Cellular protein was collected after 5 days and IDE was measured by western
527 blot. Surprisingly, overexpression of APP in *App*^{-/-} astrocytes did not significantly change IDE
528 levels (p=0.56) (Fig. 7C).

529

530 **DISCUSSION**

531

532 Glucose hypometabolism in the brain is observed in advanced Alzheimer's disease, in animal
533 models of AD, and in Down syndrome patients (45, 65, 68, 87). AD patients exhibit type-2
534 diabetes or impaired glucose tolerance at twice the rate of age-matched controls (86). A plethora
535 of evidence shows an association between type-2 diabetes and cognitive decline, but recent
536 studies have challenged the hypothesis that AD is promoted by type-2 diabetes, as the latter is
537 better correlated with vascular dementia (34, 35, 41, 55). Moreover, diabetes has not been found
538 to exacerbate A β deposition in all studies (69, 76). The converse, however, may be true, as
539 indicated by the perturbation of peripheral insulin/glucose regulation in AD models (52, 53, 62,
540 64). Most of these models involve overexpression of APP and evidence suggests the precursor
541 participates in metabolic homeostasis. For example, *App*^{-/-} knockout mice, in addition to having
542 lower body weight, show reduced weight gain compared to *App*^{+/+} controls when placed on a
543 high-fat diet (71). In muscle tissue, sAPP α potentiates glucose uptake (27). Our data
544 demonstrates that ablation of the APP gene in mice or prolonged knockdown of APP in cell
545 culture results in higher levels of IDE compared to *App*^{+/+} controls. Higher levels of IDE protein
546 were observed in muscle, liver, and hippocampal tissue extracts from *App*^{-/-} animals. In
547 agreement with this, primary cell cultures of neurons, astrocytes and microglia from *App*^{-/-} mice
548 all had elevated IDE levels compared to *App*^{+/+} cultures. Furthermore, *Ide* mRNA levels were

549 significantly increased in hippocampal tissue from *App*^{-/-} animals compared to controls,
550 suggesting that increased IDE protein was due to increased transcription. The effect seen *in vivo*
551 did not appear to result from indirect effects of developmental abnormalities because knockdown
552 of APP in cultured cells was sufficient to acutely elevate protein levels of IDE.

553

554 We observed robust and significantly higher IDE activity in both hippocampus and liver extracts
555 from *App*^{-/-} animals compared to *App*^{+/+} controls. IDE activity was not statistically different in
556 skeletal muscle tissue extracts despite increased total IDE proteins levels. This could be due to
557 the nature of the activity assay, which uses cleavage of a FRET peptide as an indicator of IDE
558 activity. Muscle tissue may contain other enzymes capable of cleaving the FRET substrate.
559 Interestingly, muscle tissue lysates had additional, lower-molecular-weight IDE bands on
560 western blots compared to other tissues, suggesting there may be alternative forms of IDE in
561 muscle or that the enzyme is subject to an unusually higher rate of proteolysis in this tissue.

562

563 Although the brain is traditionally viewed as an insulin-insensitive organ, recent literature
564 demonstrates insulin and insulin signaling are involved in the normal physiology of the brain
565 (18, 23, 40). Moreover, impaired insulin signaling may play a role in AD (75, 81). Indeed,
566 intranasal insulin is under investigation as a therapeutic intervention for AD (7). We observed
567 significantly lower hippocampal insulin levels in *App*^{-/-} animals suggesting that higher IDE
568 activity is tantamount to greater insulin catabolism. This concept is in general agreement with
569 previous research showing IDE^{-/-} mice have impaired tissue insulin degradation (17).

570

571 Our data also indicates that increased IDE protein and activity alter brain insulin signaling.
572 While we did not clearly detect phosphorylated insulin receptor in our hippocampus
573 homogenates, possibly due to the transient nature of insulin receptor phosphorylation, we did
574 observe modest but significantly reduced levels of pAKT(T308) in the *App*^{-/-} hippocampus. This
575 suggested that insulin signaling may be impaired in *App*^{-/-} brain tissues, perhaps due to lower
576 levels of insulin itself. However, we also observed diminished phosphorylation of the insulin
577 receptor following acute stimulation of *App*^{-/-} synaptosomes compared to *App*^{+/+} controls. This
578 suggests that differences in signaling in *App*^{-/-} brains may occur via receptor dysfunction as well.
579
580 To examine physiologic consequences of increased tissue levels of IDE in *App*^{-/-} mice, we
581 assessed insulin in serum. Six weeks of western diet produced hyperinsulinemia in *App*^{+/+} mice
582 but not *App*^{-/-} mice. Pharmacologic inhibition of IDE *in vivo* has been shown to alter insulin
583 levels and impair glucose tolerance (14). Consistent with this finding, elevated IDE in the *App*^{-/-}
584 mice correlated with protection against insulin resistance and glucose intolerance. It is possible
585 that suppression of circulating insulin permits the maintenance of greater insulin sensitivity in
586 *App*^{-/-} mice, which may manifest in the lower serum insulin levels observed in *App*^{-/-} mice.
587 Indeed, this is in agreement with a recent report showing that reduced pancreatic beta cell mass in
588 *App*^{-/-} mice challenged with a high fat diet (13). It should be noted that while levels of serum
589 insulin were reduced in fasted *App*^{-/-} mice, their pancreatic response to glucose showed a greater
590 dynamic response, achieving levels similar to those in *App*^{+/+} mice. This exaggerated
591 responsiveness appears to be consistent with the phenotype of isolated pancreatic islets in a
592 previous report (83). In addition to impacts on insulin, IDE may alter peripheral glucose
593 regulation through its degradation of glucagon (79). In agreement with our study, recent work by

594 Czczor et al. observed lower plasma levels of insulin in fasted *App*^{-/-} mice fed a high fat diet for
595 14 weeks (12). However, they observed that high fat diet caused glucose intolerance while
596 insulin tolerance remained normal in the *App*^{-/-} mice. The incongruity is perhaps due to the large
597 difference in sucrose composition in the diets which was 34% by mass in our “western diet”
598 study and 20% in the study by Czczor et al.

599

600 It is interesting to note that while *App*^{-/-} mice retained insulin sensitivity in the periphery when
601 placed on a western diet, they had impaired insulin signaling in the brain. The reason for this is
602 unclear. However, insulin sensitivity in tissues is affected by numerous factors, including
603 phosphorylation status of the insulin receptor substrate 1 (IRS-1), downstream of the insulin
604 receptor (11, 56). Surprisingly, hippocampal synaptosomes from *App*^{-/-} animals demonstrated
605 acute insulin resistance at the level of the insulin receptor suggesting a complex response to
606 elevated IDE in the brain. Since the brain is exposed to much lower levels of insulin than
607 peripheral organs it is not surprising that elevated IDE activity in the brain may have differential
608 consequences on tissue insulin signaling compared to the periphery. Furthermore, it is known
609 that the adult brain expresses a different isoform of the insulin receptor which has a greater
610 affinity for both insulin and IGF-II compared to the insulin receptor predominantly found in
611 peripheral tissues (2, 22, 25). This difference in central and peripheral insulin receptor isoforms
612 may further account for the apparent differential effects of increased IDE in the brain compared
613 to periphery.

614

615 To further examine the potential functional consequences of increased tissue levels of IDE in
616 aging animals, we performed glucose tolerance testing in 12 month old male and female WT and

617 *App*^{-/-} animals. Pharmacological inhibition of the IDE *in vivo* has been shown to alter insulin
618 levels and affect glucose tolerance (14). While we did not observe a significant difference in
619 overall glucose tolerance between WT and *App*^{-/-} animals, we were surprised to observe that
620 when aged *App*^{-/-} animals were fasted, they became hypoglycemic. This is in contrast to our prior
621 analysis of glucose levels in 2 month *App*^{-/-} animals, which did not reveal this phenomenon
622 despite increased levels of pancreatic IDE (42). This finding, however, is in general agreement
623 with work by Needham et al. which demonstrated lower plasma glucose in both *App*^{-/-} and
624 APLP2^{-/-} mice (63). Other groups have shown that aged *App*^{-/-} animals have impaired spatial
625 learning with age (58, 70). It can be speculated that aging may reveal phenotypes present in *App*^{-/-}
626 ^{-/-} mice not observed at earlier ages. Indeed, it has been shown that aged *App*^{-/-} mice, but not
627 young *App*^{-/-} mice, show fewer dendritic spines and changes in spine morphology in addition to
628 impaired LTP (46, 84). The compromised metabolic homeostasis we observed in aged animals
629 may reveal the potentially deleterious consequences of increased IDE in tissues, despite normal
630 overall glucose tolerance. IDE has been implicated in the degradation of the glucose elevating
631 hormone glucagon, which may account in part for this the hypoglycemia we observed in fasting
632 conditions (79).

633

634 The mechanism by which ablation of APP results in increased IDE transcription remains to be
635 elucidated. The APP intracellular domain (AICD) can interact with other proteins such as Fe65,
636 Dab1, and the histone acetyltransferase Tip60 to transduce intracellular signals (6, 39). One of
637 these accessory proteins is NEDD8, which activates ubiquitin-proteasome degradation of
638 substrates in the Cullin pathways (74). However, little is known about degradation of IDE via the
639 ubiquitin-proteasome system, and our analysis of mRNA suggests a pretranslational site of

640 action. Treatment of the SIM-A9 microglia cell line with secretase inhibitors did not significantly
641 change IDE levels, suggesting that APP processing is not necessary for the impact on IDE.
642 Previous research has indicated that APP may be able to affect transcription independently of γ -
643 secretase activity (29). Regardless, a reliance on holo-APP would not be inconsistent with
644 schemes in which both the intact precursor and one of its fragments are involved. It has been
645 suggested that sAPP α requires the APP holoprotein for its normal signaling functions (90). A
646 recent report has shown that viral overexpression of sAPP α in the brain increases IDE and
647 restores memory deficits in a mouse model for AD (20). Perhaps the increased IDE observed in
648 the *App*^{-/-} mice results from loss of normal sAPP α -APP signaling. In our study, *in vitro* treatment
649 of *App*^{-/-} astrocytes with recombinant sAPP α or sAPP β did not alter IDE protein levels; nor did
650 treatment of the SIM-A9 microglia cell line with α - or β -secretase inhibitors. It was also
651 somewhat surprising that overexpression of human APP695 or APP751 was not sufficient to
652 change IDE levels in *App*^{-/-} astrocyte cultures. This may be due to abnormal processing or
653 trafficking of the exogenous, overexpressed APP. Regardless, long-term siRNA knockdown of
654 APP *in vitro* was sufficient to robustly change IDE levels supporting our observations in the *App*^{-/-}
655 mice. It is also possible that changes in IDE occur indirectly from loss of APP instead of APP
656 being directly involved in IDE transcription.

657
658 In conclusion, we present new evidence that APP suppresses the levels of IDE mRNA, protein,
659 and enzymatic activity, both in the brain and in peripheral organs. These findings represent a
660 new link connecting APP to metabolic homeostasis and expand on the already substantial
661 connections between Alzheimer's disease and metabolism. Further, these findings may have

662 relevance for situations—empirical or otherwise—in which holo-APP is overexpressed, wherein
663 greater restriction of IDE levels may alter A β accumulation.

664

665 **Grants:** SWB and RDH were supported by NIH P01AG012411. JAK, GDM, KLP, and CKC
666 were supported by NIH R01AGO48993 and NIH RO1AGO42819 and NIH/NIGMS grant
667 P20GM113123.

668 **Disclosures:** The authors declare no competing financial interests.

669

670

671

- 673 1. **Alessi DR, Andjelkovic M, Caudwell B, Cron P, Morrice N, Cohen P, and Hemmings BA.**
674 Mechanism of activation of protein kinase B by insulin and IGF-1. *The EMBO journal* 15: 6541-6551,
675 1996.
- 676 2. **Belfiore A, Frasca F, Pandini G, Sciacca L, and Vigneri R.** Insulin receptor isoforms and insulin
677 receptor/insulin-like growth factor receptor hybrids in physiology and disease. *Endocrine reviews* 30:
678 586-623, 2009.
- 679 3. **Bradford MM.** A rapid and sensitive method for the quantitation of microgram quantities of
680 protein utilizing the principle of protein-dye binding. *Analytical biochemistry* 72: 248-254, 1976.
- 681 4. **Brewer GJ, Torricelli JR, Evege EK, and Price PJ.** Optimized survival of hippocampal neurons in
682 B27-supplemented Neurobasal, a new serum-free medium combination. *Journal of neuroscience*
683 *research* 35: 567-576, 1993.
- 684 5. **Bush AI, Pettingell WH, Jr., de Paradis M, Tanzi RE, and Wasco W.** The amyloid beta-protein
685 precursor and its mammalian homologues. Evidence for a zinc-modulated heparin-binding superfamily.
686 *The Journal of biological chemistry* 269: 26618-26621, 1994.
- 687 6. **Cao X, and Sudhof TC.** A transcriptionally [correction of transcriptively] active complex of APP
688 with Fe65 and histone acetyltransferase Tip60. *Science (New York, NY)* 293: 115-120, 2001.
- 689 7. **Chapman CD, Schioth HB, Grillo CA, and Benedict C.** Intranasal insulin in Alzheimer's disease:
690 Food for thought. *Neuropharmacology* 2017.
- 691 8. **Chen Y, Neve R, Zheng H, Griffin W, Barger S, and Mrak R.** Cycle on Wheels: Is APP Key to the
692 AppBp1 Pathway? *Austin Alzheimer's and Parkinson's disease* 1: 2014.
- 693 9. **Clarke JR, Lyra ESNM, Figueiredo CP, Frozza RL, Ledo JH, Beckman D, Katashima CK, Razolli D,**
694 **Carvalho BM, Frazao R, Silveira MA, Ribeiro FC, Bomfim TR, Neves FS, Klein WL, Medeiros R, LaFerla**
695 **FM, Carnevali JB, Saad MJ, Munoz DP, Velloso LA, Ferreira ST, and De Felice FG.** Alzheimer-
696 associated Abeta oligomers impact the central nervous system to induce peripheral metabolic
697 deregulation. *EMBO molecular medicine* 7: 190-210, 2015.
- 698 10. **Colvin BA, Rogers VA, Kulas JA, Ridgway EA, Amtashar FS, Combs CK, and Nichols MR.** The
699 conformational epitope for a new Abeta42 protofibril-selective antibody partially overlaps with the
700 peptide N-terminal region. *Journal of neurochemistry* 143: 736-749, 2017.
- 701 11. **Copps KD, Hancer NJ, Opore-Ado L, Qiu W, Walsh C, and White MF.** Irs1 serine 307 promotes
702 insulin sensitivity in mice. *Cell metabolism* 11: 84-92, 2010.
- 703 12. **Czeczor J, Genders A, Aston-Mourney K, Connor T, Hall L, Hasebe K, Ellis M, De Jong K,**
704 **Henstridge D, Meikle P, Febbraio M, Walder K, and McGee SL.** APP deficiency results in resistance to
705 obesity but impairs glucose tolerance upon high fat feeding. *The Journal of endocrinology* 2018.
- 706 13. **Czeczor JK, Genders AJ, Aston-Mourney K, Connor T, Hall LG, Hasebe K, Ellis M, De Jong KA,**
707 **Henstridge DC, Meikle PJ, Febbraio MA, Walder K, and McGee SL.** APP deficiency results in resistance
708 to obesity but impairs glucose tolerance upon high fat feeding. *The Journal of endocrinology* 237: 311-
709 322, 2018.
- 710 14. **Deprez-Poulain R, Hennuyer N, Bosc D, Liang WG, Enee E, Marechal X, Charton J,**
711 **Totobenazara J, Berte G, Jahklal J, Verdelet T, Dumont J, Dassonneville S, Woitrain E, Gauriot M,**
712 **Paquet C, Duplan I, Hermant P, Cantrelle FX, Sevin E, Culot M, Landry V, Herledan A, Piveteau C,**
713 **Lippens G, Leroux F, Tang WJ, van Endert P, Staels B, and Deprez B.** Catalytic site inhibition of insulin-
714 degrading enzyme by a small molecule induces glucose intolerance in mice. *Nature communications* 6:
715 8250, 2015.
- 716 15. **Dovey HF, John V, Anderson JP, Chen LZ, de Saint Andrieu P, Fang LY, Freedman SB, Folmer B,**
717 **Goldbach E, Holsztynska EJ, Hu KL, Johnson-Wood KL, Kennedy SL, Kholodenko D, Knops JE, Latimer**

- 718 **LH, Lee M, Liao Z, Lieberburg IM, Motter RN, Mutter LC, Nietz J, Quinn KP, Sacchi KL, Seubert PA,**
719 **Shopp GM, Thorsett ED, Tung JS, Wu J, Yang S, Yin CT, Schenk DB, May PC, Altstiel LD, Bender MH,**
720 **Boggs LN, Britton TC, Clemens JC, Czilli DL, Dieckman-McGinty DK, Droste JJ, Fuson KS, Gitter BD,**
721 **Hyslop PA, Johnstone EM, Li WY, Little SP, Mabry TE, Miller FD, and Audia JE.** Functional gamma-
722 secretase inhibitors reduce beta-amyloid peptide levels in brain. *Journal of neurochemistry* 76: 173-181,
723 2001.
- 724 16. **Duckworth WC, Bennett RG, and Hamel FG.** Insulin degradation: progress and potential.
725 *Endocrine reviews* 19: 608-624, 1998.
- 726 17. **Farris W, Mansourian S, Chang Y, Lindsley L, Eckman EA, Frosch MP, Eckman CB, Tanzi RE,**
727 **Selkoe DJ, and Guenette S.** Insulin-degrading enzyme regulates the levels of insulin, amyloid beta-
728 protein, and the beta-amyloid precursor protein intracellular domain in vivo. *Proceedings of the*
729 *National Academy of Sciences of the United States of America* 100: 4162-4167, 2003.
- 730 18. **Fernandez AM, Hernandez-Garzon E, Perez-Domper P, Perez-Alvarez A, Mederos S, Matsui T,**
731 **Santi A, Trueba-Saiz A, Garcia-Guerra L, Pose-Utrilla J, Fielitz J, Olson EN, Fernandez de la Rosa R,**
732 **Garcia Garcia L, Pozo MA, Iglesias T, Araque A, Soya H, Perea G, Martin ED, and Torres Aleman I.**
733 Insulin Regulates Astrocytic Glucose Handling Through Cooperation With IGF-I. *Diabetes* 66: 64-74, 2017.
- 734 19. **Floden AM, Li S, and Combs CK.** Beta-amyloid-stimulated microglia induce neuron death via
735 synergistic stimulation of tumor necrosis factor alpha and NMDA receptors. *The Journal of neuroscience*
736 *: the official journal of the Society for Neuroscience* 25: 2566-2575, 2005.
- 737 20. **Fol R, Braudeau J, Ludewig S, Abel T, Weyer SW, Roederer JP, Brod F, Audrain M, Bemelmans**
738 **AP, Buchholz CJ, Korte M, Cartier N, and Muller UC.** Viral gene transfer of APP α rescues synaptic
739 failure in an Alzheimer's disease mouse model. *Acta neuropathologica* 131: 247-266, 2016.
- 740 21. **Franklin W, and Tagliatela G.** A method to determine insulin responsiveness in synaptosomes
741 isolated from frozen brain tissue. *Journal of neuroscience methods* 261: 128-134, 2016.
- 742 22. **Frasca F, Pandini G, Scalia P, Sciacca L, Mineo R, Costantino A, Goldfine ID, Belfiore A, and**
743 **Vigneri R.** Insulin receptor isoform A, a newly recognized, high-affinity insulin-like growth factor II
744 receptor in fetal and cancer cells. *Molecular and cellular biology* 19: 3278-3288, 1999.
- 745 23. **Garcia-Caceres C, Quarta C, Varela L, Gao Y, Gruber T, Legutko B, Jastroch M, Johansson P,**
746 **Ninkovic J, Yi CX, Le Thuc O, Szigeti-Buck K, Cai W, Meyer CW, Pfluger PT, Fernandez AM, Luquet S,**
747 **Woods SC, Torres-Aleman I, Kahn CR, Gotz M, Horvath TL, and Tschop MH.** Astrocytic Insulin Signaling
748 Couples Brain Glucose Uptake with Nutrient Availability. *Cell* 166: 867-880, 2016.
- 749 24. **Glenner GG, and Wong CW.** Alzheimer's disease: initial report of the purification and
750 characterization of a novel cerebrovascular amyloid protein. *Biochemical and biophysical research*
751 *communications* 120: 885-890, 1984.
- 752 25. **Gray SM, and Barrett EJ.** Insulin transport into the brain. *American journal of physiology Cell*
753 *physiology* 315: C125-C136, 2018.
- 754 26. **Habib A, Sawmiller D, and Tan J.** Restoring Soluble Amyloid Precursor Protein alpha Functions
755 as a Potential Treatment for Alzheimer's Disease. *Journal of neuroscience research* 95: 973-991, 2017.
- 756 27. **Hamilton DL, Findlay JA, Montagut G, Meakin PJ, Bestow D, Jality SM, and Ashford ML.** Altered
757 amyloid precursor protein processing regulates glucose uptake and oxidation in cultured rodent
758 myotubes. *Diabetologia* 57: 1684-1692, 2014.
- 759 28. **Harris RA, Tindale L, Lone A, Singh O, Macauley SL, Stanley M, Holtzman DM, Bartha R, and**
760 **Cumming RC.** Aerobic Glycolysis in the Frontal Cortex Correlates with Memory Performance in Wild-
761 Type Mice But Not the APP/PS1 Mouse Model of Cerebral Amyloidosis. *The Journal of neuroscience : the*
762 *official journal of the Society for Neuroscience* 36: 1871-1878, 2016.
- 763 29. **Hass MR, and Yankner BA.** A γ -secretase-independent mechanism of signal transduction
764 by the amyloid precursor protein. *The Journal of biological chemistry* 280: 36895-36904, 2005.

- 765 30. **Hassing LB, Johansson B, Nilsson SE, Berg S, Pedersen NL, Gatz M, and McClearn G.** Diabetes
766 mellitus is a risk factor for vascular dementia, but not for Alzheimer's disease: a population-based study
767 of the oldest old. *International psychogeriatrics* 14: 239-248, 2002.
- 768 31. **Heber S, Herms J, Gajic V, Hainfellner J, Aguzzi A, Rulicke T, von Kretzschmar H, von Koch C,**
769 **Sisodia S, Tremml P, Lipp HP, Wolfer DP, and Muller U.** Mice with combined gene knock-outs reveal
770 essential and partially redundant functions of amyloid precursor protein family members. *The Journal of*
771 *neuroscience : the official journal of the Society for Neuroscience* 20: 7951-7963, 2000.
- 772 32. **Hoettecke N, Ludwig A, Foro S, and Schmidt B.** Improved synthesis of ADAM10 inhibitor
773 GI254023X. *Neuro-degenerative diseases* 7: 232-238, 2010.
- 774 33. **Hoyer S.** Abnormalities of glucose metabolism in Alzheimer's disease. *Annals of the New York*
775 *Academy of Sciences* 640: 53-58, 1991.
- 776 34. **Hundhausen C, Misztela D, Berkhout TA, Broadway N, Saftig P, Reiss K, Hartmann D,**
777 **Fahrenholz F, Postina R, Matthews V, Kallen KJ, Rose-John S, and Ludwig A.** The disintegrin-like
778 metalloproteinase ADAM10 is involved in constitutive cleavage of CX3CL1 (fractalkine) and regulates
779 CX3CL1-mediated cell-cell adhesion. *Blood* 102: 1186-1195, 2003.
- 780 35. **Jacobsen KT, and Iverfeldt K.** Amyloid precursor protein and its homologues: a family of
781 proteolysis-dependent receptors. *Cellular and molecular life sciences : CMLS* 66: 2299-2318, 2009.
- 782 36. **Jara JH, Singh BB, Floden AM, and Combs CK.** Tumor necrosis factor alpha stimulates NMDA
783 receptor activity in mouse cortical neurons resulting in ERK-dependent death. *Journal of neurochemistry*
784 100: 1407-1420, 2007.
- 785 37. **Kalyani RR, Golden SH, and Cefalu WT.** Diabetes and Aging: Unique Considerations and Goals of
786 Care. *Diabetes care* 40: 440-443, 2017.
- 787 38. **Kennedy ME, Stamford AW, Chen X, Cox K, Cumming JN, Dockendorf MF, Egan M, Ereshefsky**
788 **L, Hodgson RA, Hyde LA, Jhee S, Kleijn HJ, Kovelkar R, Li W, Mattson BA, Mei H, Palcza J, Scott JD,**
789 **Tanen M, Troyer MD, Tseng JL, Stone JA, Parker EM, and Forman MS.** The BACE1 inhibitor verubecestat
790 (MK-8931) reduces CNS beta-amyloid in animal models and in Alzheimer's disease patients. *Science*
791 *translational medicine* 8: 363ra150, 2016.
- 792 39. **Kimberly WT, Zheng JB, Guenette SY, and Selkoe DJ.** The intracellular domain of the beta-
793 amyloid precursor protein is stabilized by Fe65 and translocates to the nucleus in a notch-like manner.
794 *The Journal of biological chemistry* 276: 40288-40292, 2001.
- 795 40. **Kleinridders A, Ferris HA, Cai W, and Kahn CR.** Insulin action in brain regulates systemic
796 metabolism and brain function. *Diabetes* 63: 2232-2243, 2014.
- 797 41. **Kohjima M, Sun Y, and Chan L.** Increased food intake leads to obesity and insulin resistance in
798 the tg2576 Alzheimer's disease mouse model. *Endocrinology* 151: 1532-1540, 2010.
- 799 42. **Kulas JA, Puig KL, and Combs CK.** Amyloid precursor protein in pancreatic islets. *The Journal of*
800 *endocrinology* 235: 49-67, 2017.
- 801 43. **Kurauti MA, Costa-Junior JM, Ferreira SM, Santos GJ, Sponton CHG, Carneiro EM, Telles GD,**
802 **Chacon-Mikahil MPT, Cavaglieri CR, Rezende LF, and Boschero AC.** Interleukin-6 increases the
803 expression and activity of insulin-degrading enzyme. *Scientific reports* 7: 46750, 2017.
- 804 44. **Kurochkin IV, Guarnera E, and Berezovsky IN.** Insulin-Degrading Enzyme in the Fight against
805 Alzheimer's Disease. *Trends in pharmacological sciences* 39: 49-58, 2018.
- 806 45. **Lao PJ, Handen BL, Betthausen TJ, Mihaila I, Hartley SL, Cohen AD, Tudorascu DL, Bulova PD,**
807 **Lopresti BJ, Tumuluru RV, Murali D, Mathis CA, Barnhart TE, Stone CK, Price JC, Devenny DA, Johnson**
808 **SC, Klunk WE, and Christian BT.** Alzheimer-Like Pattern of Hypometabolism Emerges with Elevated
809 Amyloid-beta Burden in Down Syndrome. *Journal of Alzheimer's disease : JAD* 61: 631-644, 2018.
- 810 46. **Lee KJ, Moussa CE, Lee Y, Sung Y, Howell BW, Turner RS, Pak DT, and Hoe HS.** Beta amyloid-
811 independent role of amyloid precursor protein in generation and maintenance of dendritic spines.
812 *Neuroscience* 169: 344-356, 2010.

- 813 47. **Lee YH, Martin JM, Maple RL, Tharp WG, and Pratley RE.** Plasma amyloid-beta peptide levels
814 correlate with adipocyte amyloid precursor protein gene expression in obese individuals.
815 *Neuroendocrinology* 90: 383-390, 2009.
- 816 48. **Lee YH, Tharp WG, Maple RL, Nair S, Permana PA, and Pratley RE.** Amyloid precursor protein
817 expression is upregulated in adipocytes in obesity. *Obesity (Silver Spring, Md)* 16: 1493-1500, 2008.
- 818 49. **Lorent K, Overbergh L, Moechars D, De Strooper B, Van Leuven F, and Van den Berghe H.**
819 Expression in mouse embryos and in adult mouse brain of three members of the amyloid precursor
820 protein family, of the alpha-2-macroglobulin receptor/low density lipoprotein receptor-related protein
821 and of its ligands apolipoprotein E, lipoprotein lipase, alpha-2-macroglobulin and the 40,000 molecular
822 weight receptor-associated protein. *Neuroscience* 65: 1009-1025, 1995.
- 823 50. **Ludwig A, Hundhausen C, Lambert MH, Broadway N, Andrews RC, Bickett DM, Leesnitzer MA,
824 and Becherer JD.** Metalloproteinase inhibitors for the disintegrin-like metalloproteinases ADAM10 and
825 ADAM17 that differentially block constitutive and phorbol ester-inducible shedding of cell surface
826 molecules. *Combinatorial chemistry & high throughput screening* 8: 161-171, 2005.
- 827 51. **Macauley SL, Stanley M, Caesar EE, Yamada SA, Raichle ME, Perez R, Mahan TE, Sutphen CL,
828 and Holtzman DM.** Hyperglycemia modulates extracellular amyloid-beta concentrations and neuronal
829 activity in vivo. *The Journal of clinical investigation* 125: 2463-2467, 2015.
- 830 52. **Macklin L, Griffith CM, Cai Y, Rose GM, Yan XX, and Patrylo PR.** Glucose tolerance and insulin
831 sensitivity are impaired in APP/PS1 transgenic mice prior to amyloid plaque pathogenesis and cognitive
832 decline. *Experimental gerontology* 88: 9-18, 2017.
- 833 53. **Maianti JP, McFedries A, Foda ZH, Kleiner RE, Du XQ, Leissring MA, Tang WJ, Charron MJ,
834 Seeliger MA, Saghatelyan A, and Liu DR.** Anti-diabetic activity of insulin-degrading enzyme inhibitors
835 mediated by multiple hormones. *Nature* 511: 94-98, 2014.
- 836 54. **Manocha GD, Floden AM, Rausch K, Kulas JA, McGregor BA, Rojanathammanee L, Puig KR,
837 Puig KL, Karki S, Nichols MR, Darland DC, Porter JE, and Combs CK.** APP Regulates Microglial Phenotype
838 in a Mouse Model of Alzheimer's Disease. *The Journal of neuroscience : the official journal of the Society
839 for Neuroscience* 36: 8471-8486, 2016.
- 840 55. **Matioli M, Suemoto CK, Rodriguez RD, Farias DS, da Silva MM, Leite REP, Ferretti-Rebustini
841 REL, Pasqualucci CA, Jacob WF, Grinberg LT, and Nitrini R.** Association between diabetes and causes of
842 dementia: Evidence from a clinicopathological study. *Dementia & neuropsychologia* 11: 406-412, 2017.
- 843 56. **Morino K, Neschen S, Bilz S, Sono S, Tsigotis D, Reznick RM, Moore I, Nagai Y, Samuel Y,
844 Sebastian D, White M, Philbrick W, and Shulman GI.** Muscle-specific IRS-1 Ser->Ala transgenic mice are
845 protected from fat-induced insulin resistance in skeletal muscle. *Diabetes* 57: 2644-2651, 2008.
- 846 57. **Mosconi L, Sorbi S, de Leon MJ, Li Y, Nacmias B, Myoung PS, Tsui W, Ginestroni A, Bessi V,
847 Fayyaz M, Caffarra P, and Pupi A.** Hypometabolism exceeds atrophy in presymptomatic early-onset
848 familial Alzheimer's disease. *Journal of nuclear medicine : official publication, Society of Nuclear
849 Medicine* 47: 1778-1786, 2006.
- 850 58. **Muller U, Cristina N, Li ZW, Wolfer DP, Lipp HP, Rulicke T, Brandner S, Aguzzi A, and
851 Weissmann C.** Behavioral and anatomical deficits in mice homozygous for a modified beta-amyloid
852 precursor protein gene. *Cell* 79: 755-765, 1994.
- 853 59. **Muller UC, and Zheng H.** Physiological functions of APP family proteins. *Cold Spring Harbor
854 perspectives in medicine* 2: a006288, 2012.
- 855 60. **Nagamoto-Combs K, Kulas J, and Combs CK.** A novel cell line from spontaneously immortalized
856 murine microglia. *Journal of neuroscience methods* 233: 187-198, 2014.
- 857 61. **Nagamoto-Combs K, Manocha GD, Puig K, and Combs CK.** An improved approach to align and
858 embed multiple brain samples in a gelatin-based matrix for simultaneous histological processing. *Journal
859 of neuroscience methods* 261: 155-160, 2016.

- 860 62. **Nalivaeva NN, Beckett C, Belyaev ND, and Turner AJ.** Are amyloid-degrading enzymes viable
861 therapeutic targets in Alzheimer's disease? *Journal of neurochemistry* 120 Suppl 1: 167-185, 2012.
- 862 63. **Needham BE, Wlodek ME, Ciccotosto GD, Fam BC, Masters CL, Proietto J, Andrikopoulos S, and**
863 **Cappai R.** Identification of the Alzheimer's disease amyloid precursor protein (APP) and its homologue
864 APLP2 as essential modulators of glucose and insulin homeostasis and growth. *The Journal of pathology*
865 215: 155-163, 2008.
- 866 64. **Niwano H, Embury PB, Greenberg BD, and Ratnoff OD.** Inhibitory action of amyloid precursor
867 protein against human Hageman factor (factor XII). *The Journal of laboratory and clinical medicine* 125:
868 251-256, 1995.
- 869 65. **Oh H, Madison C, Baker S, Rabinovici G, and Jagust W.** Dynamic relationships between age,
870 amyloid-beta deposition, and glucose metabolism link to the regional vulnerability to Alzheimer's
871 disease. *Brain : a journal of neurology* 139: 2275-2289, 2016.
- 872 66. **Oliveira FF, Almeida SS, Chen ES, Smith MC, Naffah-Mazzacoratti MDG, and Bertolucci PHF.**
873 Lifetime Risk Factors for Functional and Cognitive Outcomes in Patients with Alzheimer's Disease.
874 *Journal of Alzheimer's disease : JAD* 2018.
- 875 67. **Pacifici M, and Peruzzi F.** Isolation and culture of rat embryonic neural cells: a quick protocol.
876 *Journal of visualized experiments : JoVE* e3965, 2012.
- 877 68. **Parent MJ, Zimmer ER, Shin M, Kang MS, Fonov VS, Mathieu A, Aliaga A, Kostikov A, Do Carmo**
878 **S, Dea D, Poirier J, Soucy JP, Gauthier S, Cuello AC, and Rosa-Neto P.** Multimodal Imaging in Rat Model
879 Recapitulates Alzheimer's Disease Biomarkers Abnormalities. *The Journal of neuroscience : the official*
880 *journal of the Society for Neuroscience* 37: 12263-12271, 2017.
- 881 69. **Peila R, Rodriguez BL, and Launer LJ.** Type 2 diabetes, APOE gene, and the risk for dementia and
882 related pathologies: The Honolulu-Asia Aging Study. *Diabetes* 51: 1256-1262, 2002.
- 883 70. **Phinney AL, Calhoun ME, Wolfer DP, Lipp HP, Zheng H, and Jucker M.** No hippocampal neuron
884 or synaptic bouton loss in learning-impaired aged beta-amyloid precursor protein-null mice.
885 *Neuroscience* 90: 1207-1216, 1999.
- 886 71. **Puig KL, Brose SA, Zhou X, Sens MA, Combs GF, Jensen MD, Golovko MY, and Combs CK.**
887 Amyloid precursor protein modulates macrophage phenotype and diet-dependent weight gain. *Scientific*
888 *reports* 7: 43725, 2017.
- 889 72. **Puig KL, Floden AM, Adhikari R, Golovko MY, and Combs CK.** Amyloid precursor protein and
890 proinflammatory changes are regulated in brain and adipose tissue in a murine model of high fat diet-
891 induced obesity. *PLoS one* 7: e30378, 2012.
- 892 73. **Puig KL, Kulas JA, Franklin W, Rakoczy SG, Tagliavola G, Brown-Borg HM, and Combs CK.** The
893 Ames dwarf mutation attenuates Alzheimer's disease phenotype of APP/PS1 mice. *Neurobiology of*
894 *aging* 40: 22-40, 2016.
- 895 74. **Raffaitin C, Gin H, Empana JP, Helmer C, Berr C, Tzourio C, Portet F, Dartigues JF, Alperovitch**
896 **A, and Barberger-Gateau P.** Metabolic syndrome and risk for incident Alzheimer's disease or vascular
897 dementia: the Three-City Study. *Diabetes care* 32: 169-174, 2009.
- 898 75. **Ribe EM, and Lovestone S.** Insulin signalling in Alzheimer's disease and diabetes: from
899 epidemiology to molecular links. *Journal of internal medicine* 280: 430-442, 2016.
- 900 76. **Roberts RO, Knopman DS, Cha RH, Mielke MM, Pankratz VS, Boeve BF, Kantarci K, Geda YE,**
901 **Jack CR, Jr., Petersen RC, and Lowe VJ.** Diabetes and elevated hemoglobin A1c levels are associated
902 with brain hypometabolism but not amyloid accumulation. *Journal of nuclear medicine : official*
903 *publication, Society of Nuclear Medicine* 55: 759-764, 2014.
- 904 77. **Selkoe DJ, and Hardy J.** The amyloid hypothesis of Alzheimer's disease at 25 years. *EMBO*
905 *molecular medicine* 8: 595-608, 2016.
- 906 78. **Selkoe DJ, Podlisny MB, Joachim CL, Vickers EA, Lee G, Fritz LC, and Oltersdorf T.** Beta-amyloid
907 precursor protein of Alzheimer disease occurs as 110- to 135-kilodalton membrane-associated proteins

908 in neural and nonneural tissues. *Proceedings of the National Academy of Sciences of the United States of*
909 *America* 85: 7341-7345, 1988.

910 79. **Shen Y, Joachimiak A, Rosner MR, and Tang WJ.** Structures of human insulin-degrading enzyme
911 reveal a new substrate recognition mechanism. *Nature* 443: 870-874, 2006.

912 80. **Steen E, Terry BM, Rivera EJ, Cannon JL, Neely TR, Tavares R, Xu XJ, Wands JR, and de la**
913 **Monte SM.** Impaired insulin and insulin-like growth factor expression and signaling mechanisms in
914 Alzheimer's disease--is this type 3 diabetes? *Journal of Alzheimer's disease : JAD* 7: 63-80, 2005.

915 81. **Talbot K, Wang HY, Kazi H, Han LY, Bakshi KP, Stucky A, Fuino RL, Kawaguchi KR, Samoyedny**
916 **AJ, Wilson RS, Arvanitakis Z, Schneider JA, Wolf BA, Bennett DA, Trojanowski JQ, and Arnold SE.**
917 Demonstrated brain insulin resistance in Alzheimer's disease patients is associated with IGF-1 resistance,
918 IRS-1 dysregulation, and cognitive decline. *The Journal of clinical investigation* 122: 1316-1338, 2012.

919 82. **Tharp WG, and Sarkar IN.** Origins of amyloid-beta. *BMC genomics* 14: 290, 2013.

920 83. **Tu Z, Keller MP, Zhang C, Rabaglia ME, Greenawalt DM, Yang X, Wang IM, Dai H, Bruss MD,**
921 **Lum PY, Zhou YP, Kemp DM, Kendziorowski C, Yandell BS, Attie AD, Schadt EE, and Zhu J.** Integrative
922 analysis of a cross-loci regulation network identifies App as a gene regulating insulin secretion from
923 pancreatic islets. *PLoS genetics* 8: e1003107, 2012.

924 84. **Tyan SH, Shih AY, Walsh JJ, Maruyama H, Sarsoza F, Ku L, Eggert S, Hof PR, Koo EH, and**
925 **Dickstein DL.** Amyloid precursor protein (APP) regulates synaptic structure and function. *Molecular and*
926 *cellular neurosciences* 51: 43-52, 2012.

927 85. **Van Nostrand WE, Farrow JS, Wagner SL, Bhasin R, Goldgaber D, Cotman CW, and**
928 **Cunningham DD.** The predominant form of the amyloid beta-protein precursor in human brain is
929 protease nexin 2. *Proceedings of the National Academy of Sciences of the United States of America* 88:
930 10302-10306, 1991.

931 86. **Wijesekara N, Goncalves da Silva RA, De Felice FG, and Fraser PE.** Impaired peripheral glucose
932 homeostasis and Alzheimer's disease. *Neuropharmacology* 2017.

933 87. **Xu J, Begley P, Church SJ, Patassini S, McHarg S, Kureishy N, Hollywood KA, Waldvogel HJ, Liu**
934 **H, Zhang S, Lin W, Herholz K, Turner C, Synek BJ, Curtis MA, Rivers-Auty J, Lawrence CB, Kellett KA,**
935 **Hooper NM, Vardy ER, Wu D, Unwin RD, Faull RL, Dowsey AW, and Cooper GJ.** Elevation of brain
936 glucose and polyol-pathway intermediates with accompanying brain-copper deficiency in patients with
937 Alzheimer's disease: metabolic basis for dementia. *Scientific reports* 6: 27524, 2016.

938 88. **Yfanti C, Mengele K, Gkazepis A, Weirich G, Giersig C, Kuo WL, Tang WJ, Rosner M, and**
939 **Schmitt M.** Expression of metalloprotease insulin-degrading enzyme insulysin in normal and malignant
940 human tissues. *International journal of molecular medicine* 22: 421-431, 2008.

941 89. **Young-Pearse TL, Bai J, Chang R, Zheng JB, LoTurco JJ, and Selkoe DJ.** A critical function for
942 beta-amyloid precursor protein in neuronal migration revealed by in utero RNA interference. *The*
943 *Journal of neuroscience : the official journal of the Society for Neuroscience* 27: 14459-14469, 2007.

944 90. **Young-Pearse TL, Chen AC, Chang R, Marquez C, and Selkoe DJ.** Secreted APP regulates the
945 function of full-length APP in neurite outgrowth through interaction with integrin beta1. *Neural*
946 *development* 3: 15, 2008.

947 91. **Zhang Y, Chen K, Sloan SA, Bennett ML, Scholze AR, O'Keefe S, Phatnani HP, Guarnieri P,**
948 **Caneda C, Ruderisch N, Deng S, Liddelow SA, Zhang C, Daneman R, Maniatis T, Barres BA, and Wu JQ.**
949 An RNA-sequencing transcriptome and splicing database of glia, neurons, and vascular cells of the
950 cerebral cortex. *The Journal of neuroscience : the official journal of the Society for Neuroscience* 34:
951 11929-11947, 2014.

952 92. **Zheng H, Jiang M, Trumbauer ME, Sirinathsinghji DJ, Hopkins R, Smith DW, Heavens RP,**
953 **Dawson GR, Boyce S, Conner MW, Stevens KA, Slunt HH, Sisoda SS, Chen HY, and Van der Ploeg LH.**
954 beta-Amyloid precursor protein-deficient mice show reactive gliosis and decreased locomotor activity.
955 *Cell* 81: 525-531, 1995.

956

957

958

Table 1: Insulin levels at 6 weeks on western diet

Mouse group		[insulin] (ng/ml)		
Genotype	Diet ¹	T ₀	T ₃₀ ²	%Δ ³
App ^{+/+}	ND	0.355 ± 0.0823	0.680 ± 0.0930	111.7 ± 78.04
	WD	1.990 ± 0.107	2.077 ± 0.0947	7.07 ± 33.34
App ^{-/-}	ND	0.111 ± 0.0354	0.466 ± 0.0386 ^{††}	699.7 ± 292.0*
	WD	0.289 ± 0.0567*	0.627 ± 0.0591 [†]	160.0 ± 55.18

¹ND (Normal Diet), WD (Western Diet)

²30 min after challenge with glucose (2 g/kg body wt.)

³Group mean of the percent changes calculated for each mouse

[†]p≤0.05, ^{††}p≤0.01 vs. T₀; *p≤0.05 vs. App^{+/+} counterpart

959

960

961

962

963

964

965

966

967

968

969

970

971 **FIGURE LEGENDS**

972 **Figure 1.** IDE was increased in *App*^{-/-} tissues. **A-C**, IDE protein was measured in liver (n=7),
973 gastrocnemius (n=6), and hippocampal tissue (n=6-7) by western blot and normalized to
974 GAPDH as a loading control. Normalized optical density is graphed as mean values ±SEM. **D**,
975 *Ide* mRNA levels were measured in hippocampus extracts (n=4-5) and normalized to ribosomal
976 18S RNA as a loading control. Statistical significance p<0.05* was determined by Student's t-
977 test. **E**, Immunohistochemistry for IDE protein was performed on *App*^{+/+} and *App*^{-/-} brain tissue
978 sections (n=4-6). Representative images at 10X magnification are shown.

979

980 **Figure 2.** IDE was increased in *App*^{-/-} cell cultures. **A-C**, Primary cell cultures of neurons (n=4),
981 astrocytes (n=3), and microglia from *App*^{+/+}, *App*^{-/-} and the APP/PS1 mouse model of AD were
982 grown and assessed for IDE protein content by western blot with GAPDH as a loading control.
983 Significance p<0.05* was determined by Student's t-test. **D**, Cultures of SIM-A9 mouse
984 microglia cells (n=6/condition) were treated with either scrambled RNA or anti-APP siRNA for
985 one week. After treatment, total cellular IDE content was assessed by western blot with α-tubulin
986 as a loading control. Significance p<0.05* was determined by Student's t-test. Normalized
987 optical density is graphed as mean values ± SEM.

988

989 **Figure 3.** IDE activity was increased in *App*^{-/-} tissues. *App*^{+/+} and *App*^{-/-} tissues (n=6) were
990 harvested on ice and rapidly assayed for IDE activity over the course of 1 h. The IDE activity
991 assay uses a FRET peptide which is liberated from a quencher and exhibits increased
992 fluorescence when cleaved by IDE. Relative fluorescent units are converted to concentrations of

993 FAM via standard curve. The data was normalized to the amount of total protein collected from
994 each tissue. IDE activity was calculated from each animal tissue and significance $p < 0.05^*$ was
995 determined by Student's t-test. Data is graphed as mean values \pm SEM.

996

997 **Figure 4.** Insulin signaling and total insulin levels were altered in the *App*^{-/-} brain. **A**, Total
998 hippocampal insulin levels were measured in RIPA extractions of *App*^{+/+} and *App*^{-/-} hippocampus
999 tissue by ELISA (n=13). **B**, Insulin signaling cascade markers were assessed by western blot in
1000 two-month old *App*^{+/+} and *App*^{-/-} hippocampal tissue (n=5-6/condition). **C**, Hippocampal
1001 synaptosomes from 2 month old *App*^{+/+} and *App*^{-/-} animals were prepared and stimulated with 10
1002 nM insulin (n=5/5) or 200 nM insulin (n=6/4). pIR, total IR and β tubulin protein levels were
1003 measured using the WES system. Data was collected using the area under the peak for the
1004 specified proteins, and analysis performed using a Student's t-test with significance $p < 0.05^*$.
1005 Data is graphed as mean values \pm SEM.

1006

1007 **Figure 5.** *App*^{-/-} mice maintain glucose tolerance on a western diet. *App*^{+/+} or *App*^{-/-} mice were
1008 maintained on normal (ND) or western diet (WD). **A**, GTT at 7 weeks on diet (** $p < 0.01$,
1009 *** $p < 0.001$, *App*^{+/+} WD vs. *App*^{-/-} WD at the indicated time points; ## $p < 0.01$, *App*^{+/+} WD vs.
1010 *App*^{+/+} ND). **B**, Mean of GTTs performed during weeks 13-19 on diet, expressed as area under
1011 the curve, zeroed to the initial [GTT]_b for each mouse.. (** $p < 0.01$, *** $p < 0.001$). **C**, [Glc]_b in
1012 response to insulin at 8 weeks on diet (* $p < 0.05$, ** $p < 0.01$, *App*^{+/+} WD vs. *App*^{-/-} WD at the
1013 indicated time points; ## $p < 0.01$, *App*^{+/+} WD vs. *App*^{+/+} ND). **D**, Mean of ITTs performed during

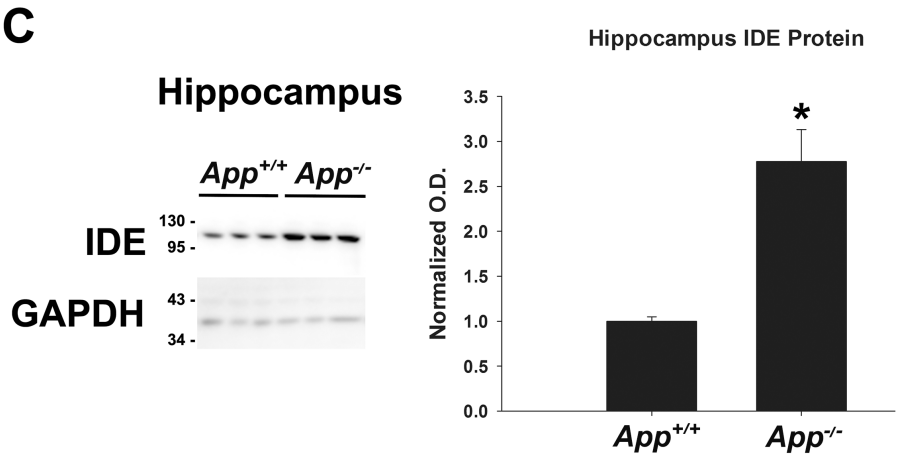
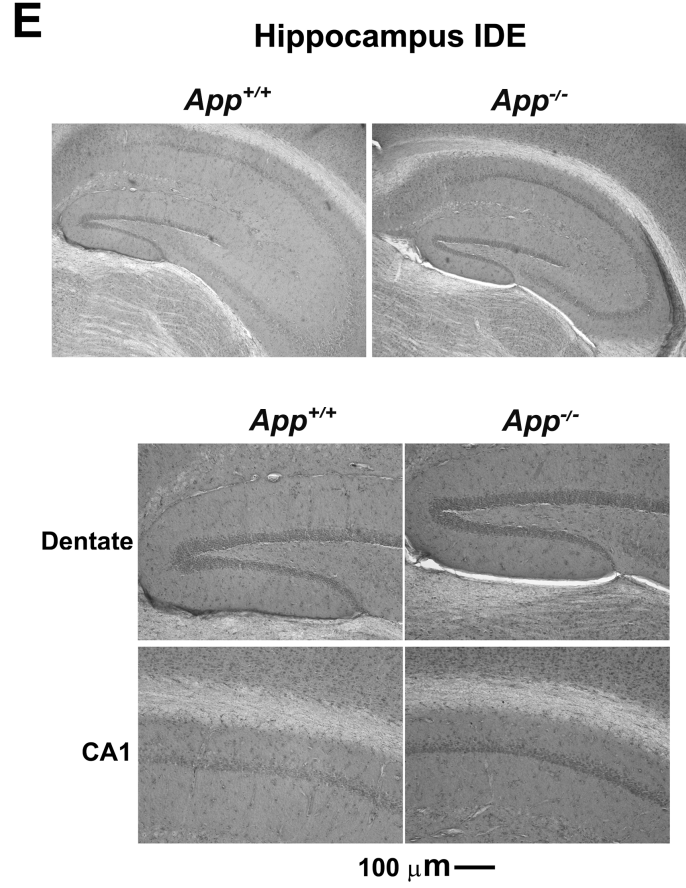
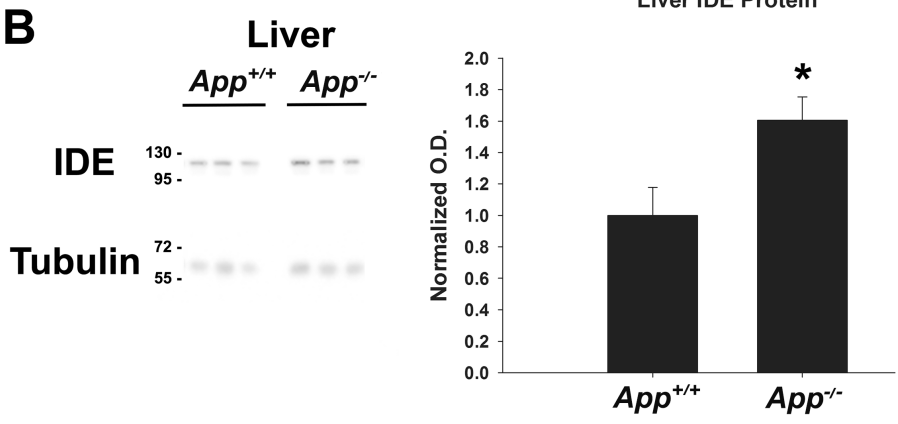
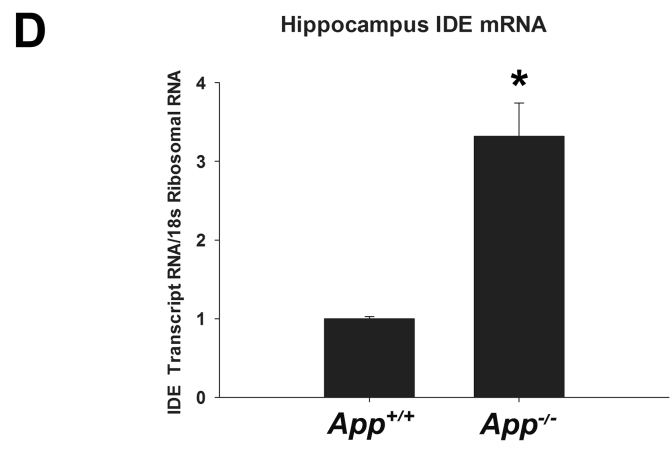
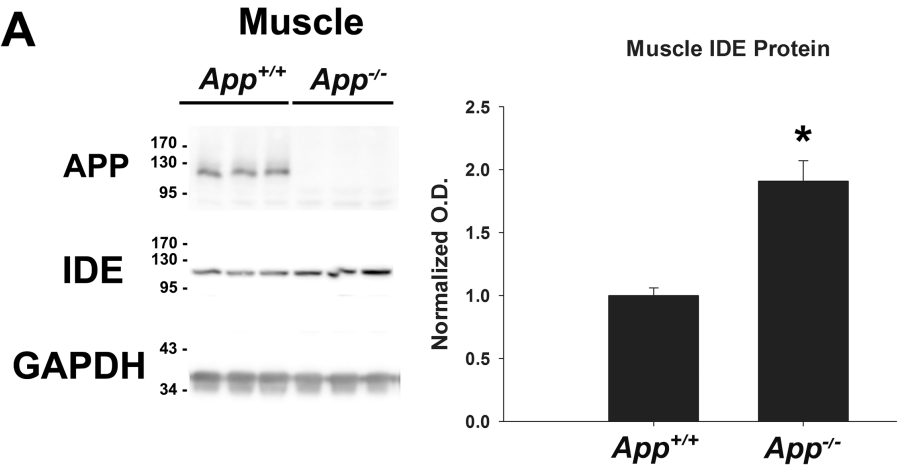
1014 weeks 12-18 on diet, expressed as area over the curve, capped at the initial [Glc]_b for each mouse
1015 (*p<0.05).

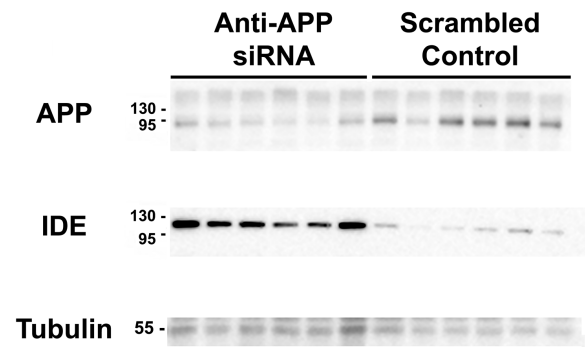
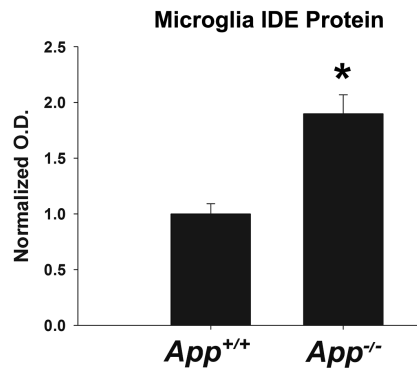
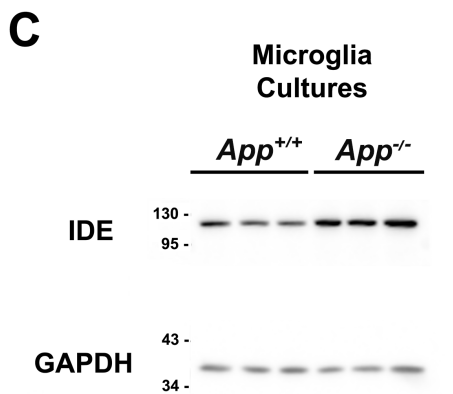
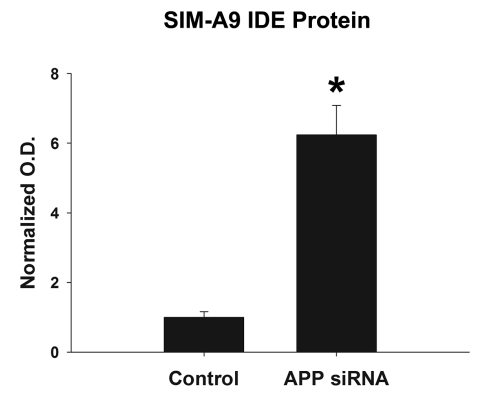
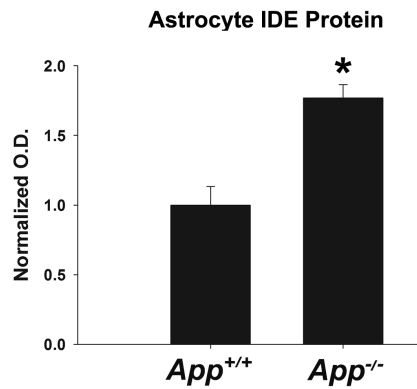
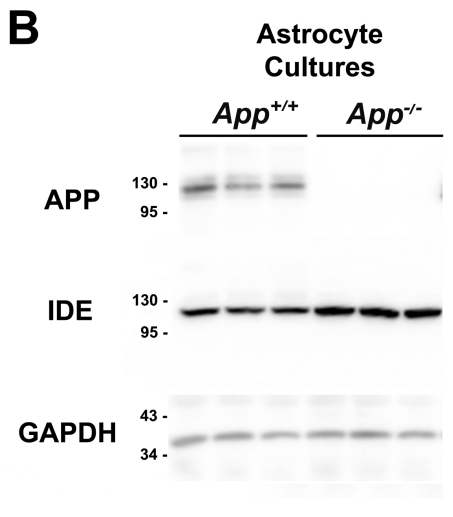
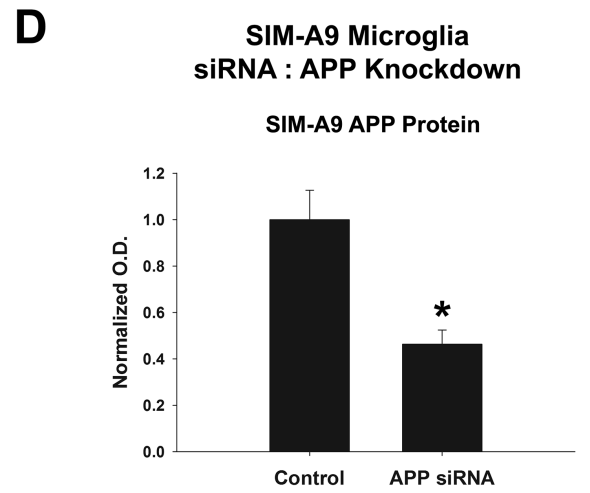
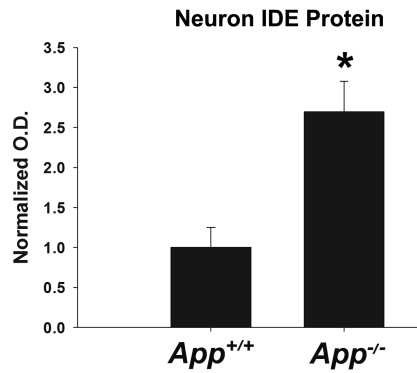
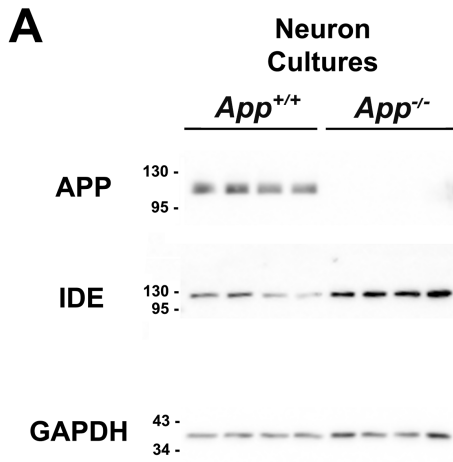
1016

1017 **Figure 6.** Aged *App*^{-/-} animals are hypoglycemic when fasted. Twelve-month-old *App*^{+/+} and
1018 *App*^{-/-} mice (n=11-13) were fasted and subjected to glucose tolerance testing with IP injections
1019 glucose. Area under the curve (AUC) was measured for each animal's blood glucose over time,
1020 and *App*^{+/+} and *App*^{-/-} animals were compared by Student's t-test with p<0.05*. Blood glucose
1021 was measured and graphed in free fed (n=5) *App*^{+/+} and *App*^{-/-} mice. Significance p<0.05* was
1022 determined by Student's t-test. Data is graphed as mean values ± SEM.

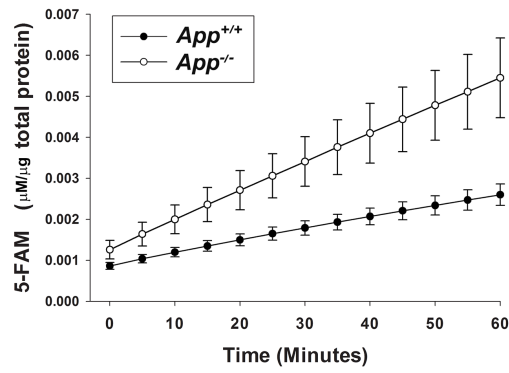
1023

1024 **Figure 7.** APP fragments, APP overexpression, and secretase inhibitors did not alter IDE in *App*^{-/-}
1025 ^{-/-} cells. **A**, SIMA9 microglia (n=3/condition) were treated with secretase inhibitors, DMSO
1026 vehicle, or left untreated for one week and IDE protein content was measured. Significance
1027 p<0.05* was determined by one-way ANOVA. **B**, *App*^{-/-} primary astrocyte cultures
1028 (n=4/condition) were treated with bacterial recombinant sAPP α , sAPP β , mutant N-terminal
1029 sAPP α or eukaryotic-derived sAPP α 695 and 751. IDE protein was measured and significance
1030 p<0.05* was determined by one-way ANOVA. **C**, *App*^{-/-} astrocyte primary cultures
1031 (n=6/condition) were transfected with APP695, APP751 or GFP plasmids or mock transfected.
1032 IDE protein was measured and significance p<0.05* was determined by one-way ANOVA. Data
1033 is graphed as mean values ± SEM.

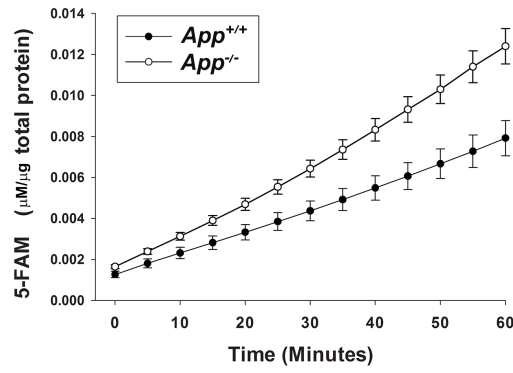




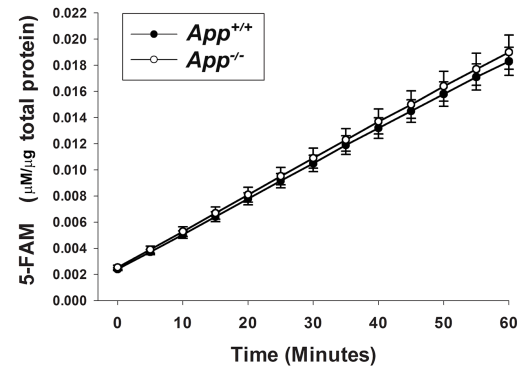
Hippocampus IDE Activity



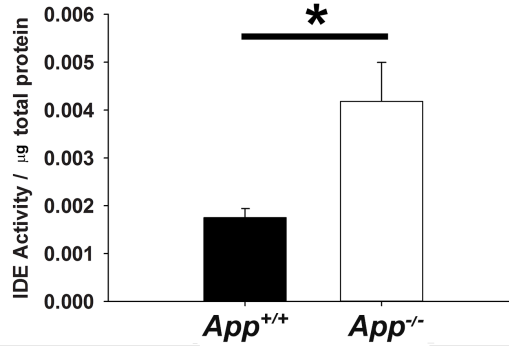
Liver IDE Activity



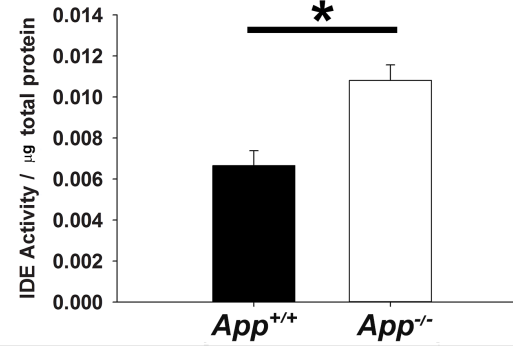
Muscle IDE Activity



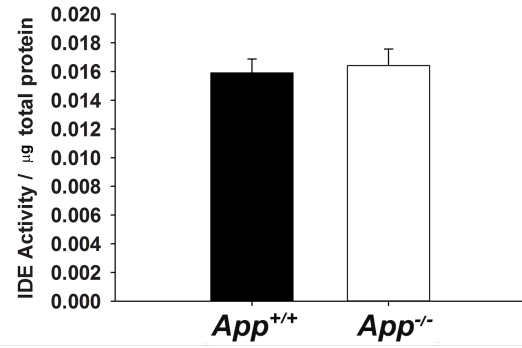
IDE Activity - Hippocampus



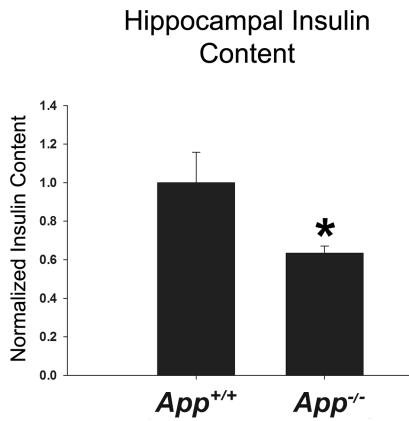
IDE Activity - Liver



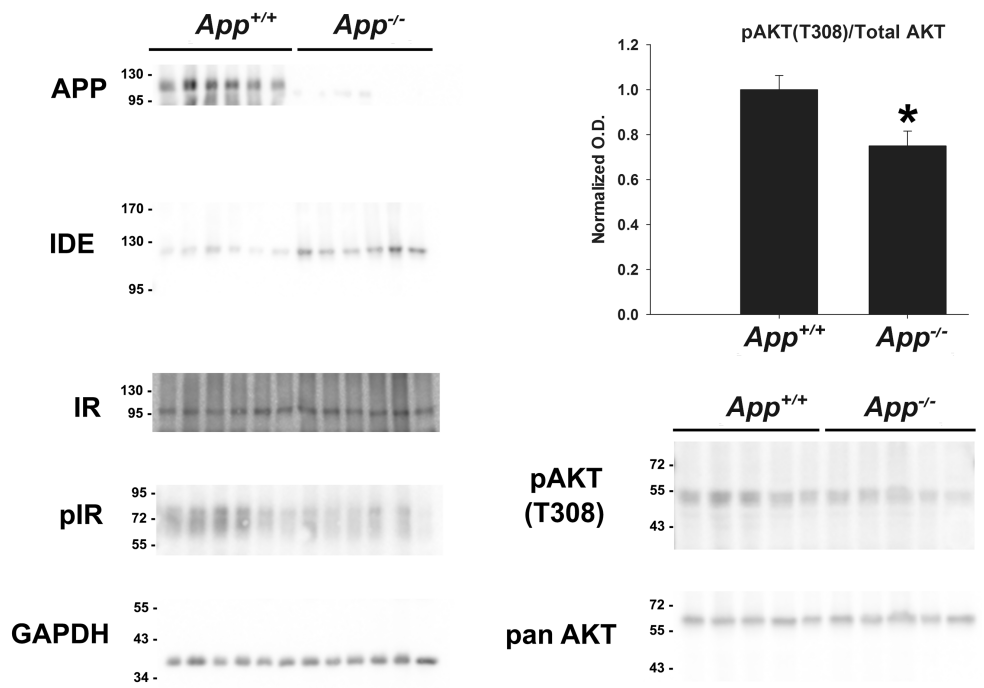
IDE Activity - Muscle



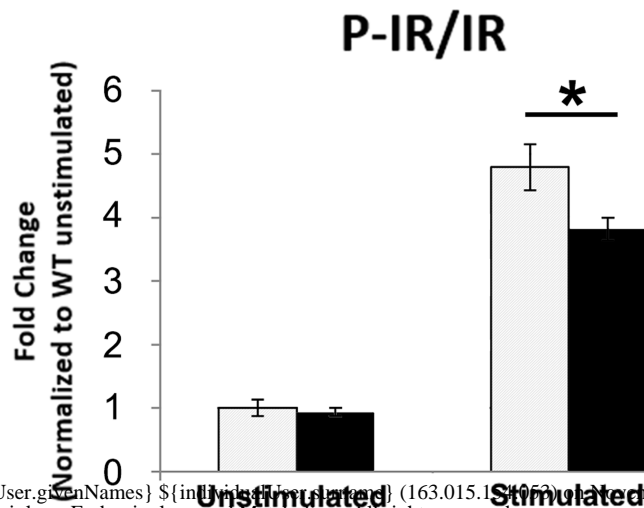
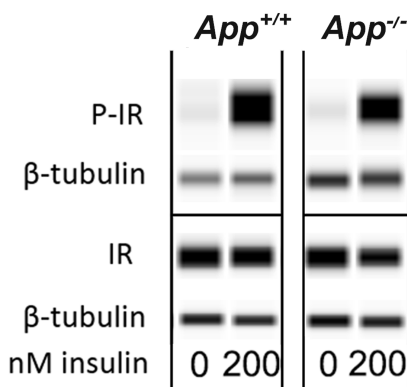
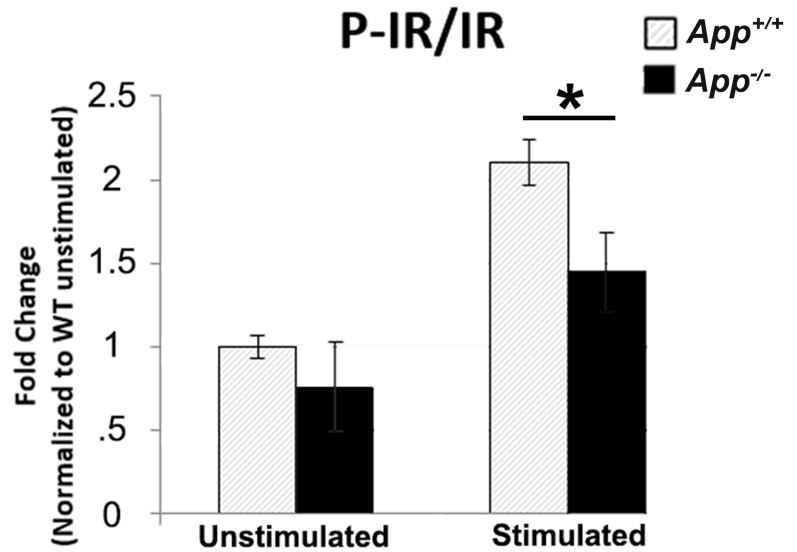
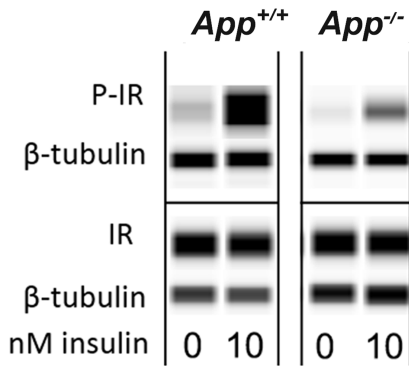
A Insulin Content

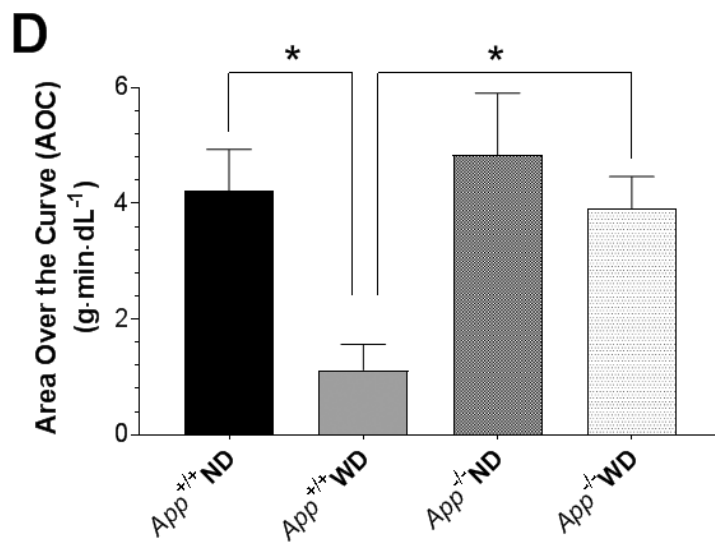
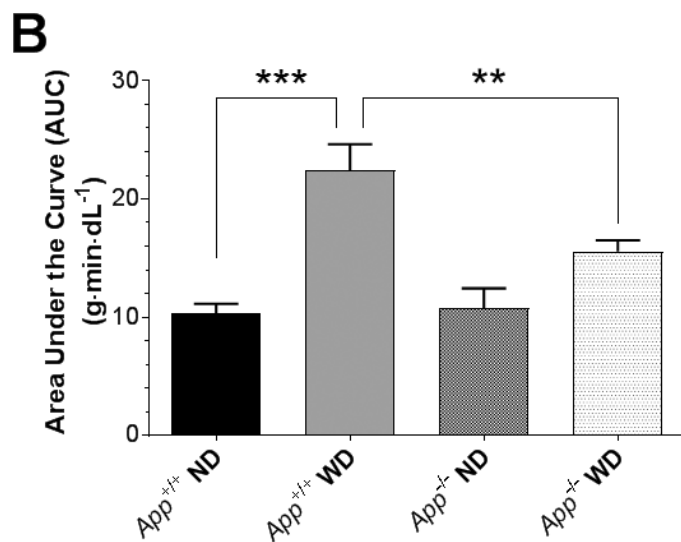
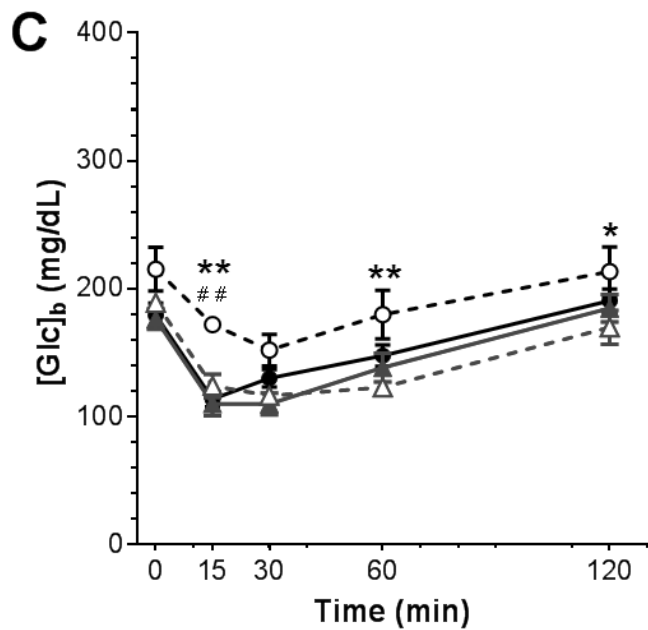
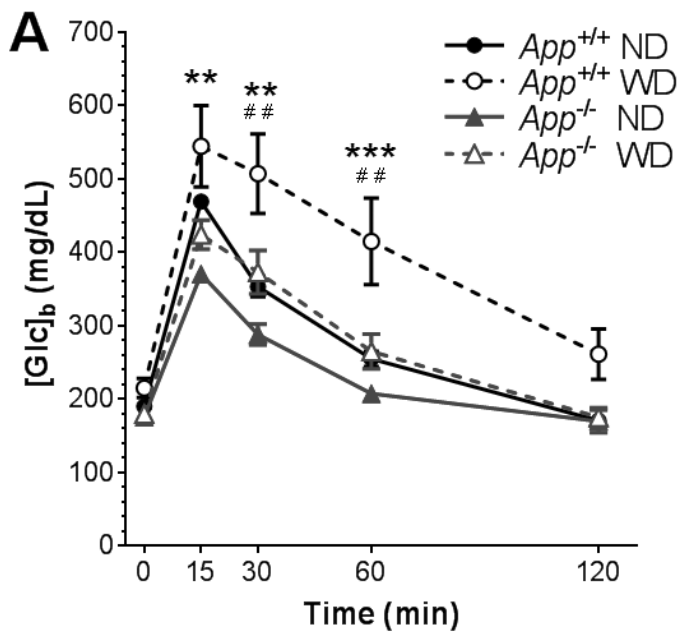


B Hippocampus Lysate

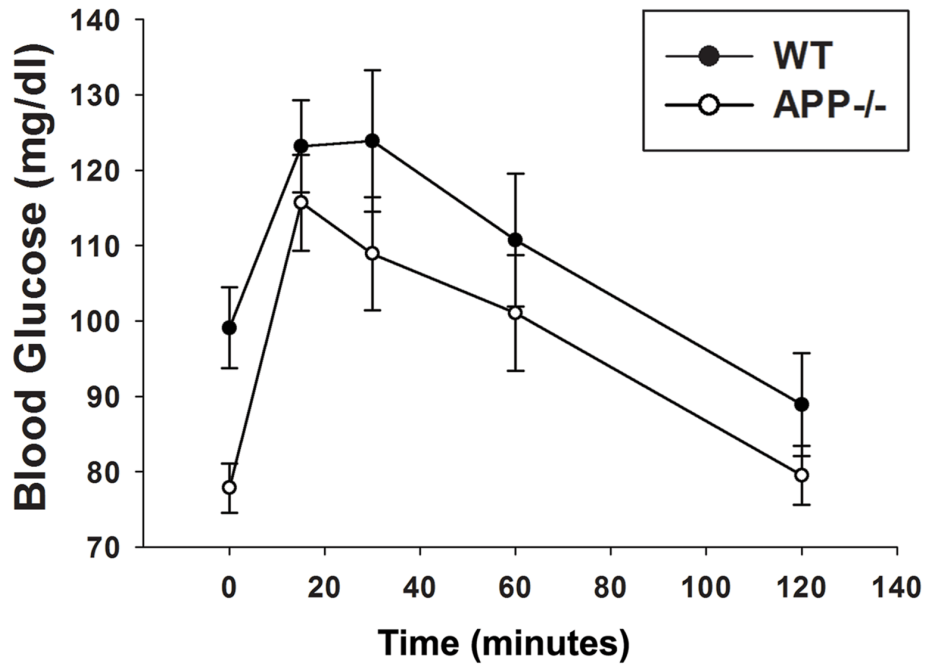


C Synaptosome Stimulations

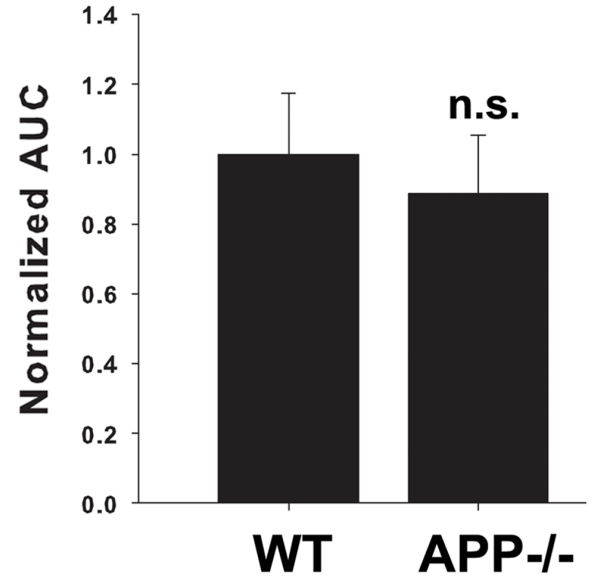




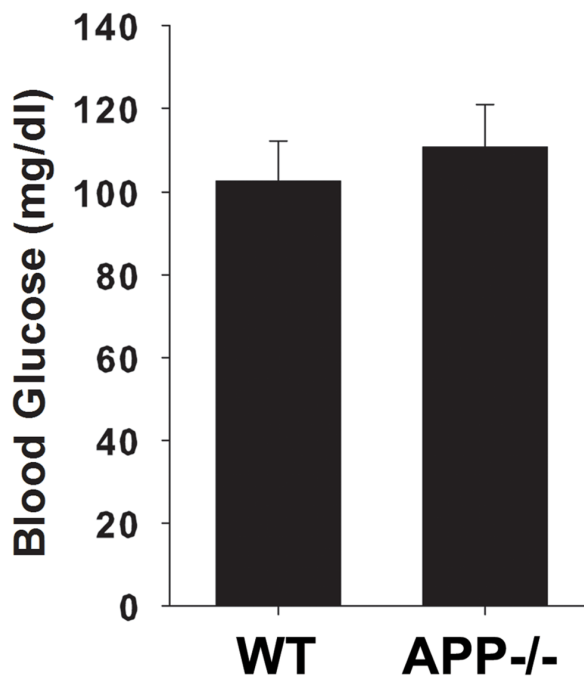
Glucose Tolerance



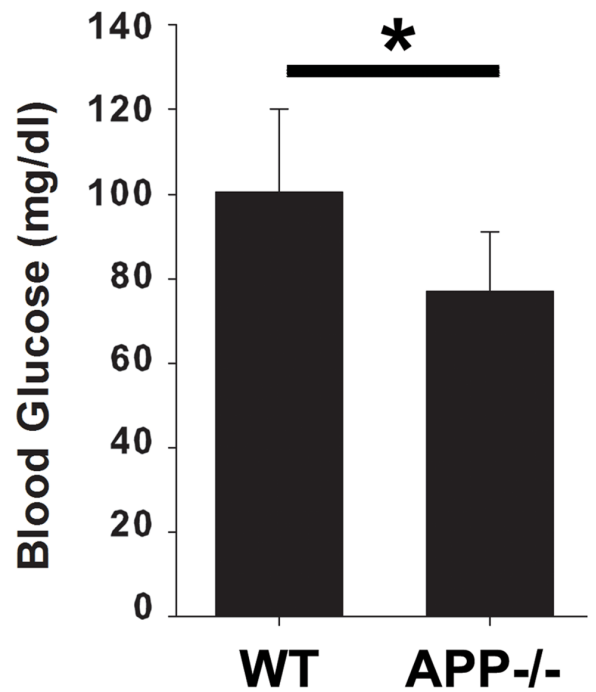
Glucose Tolerance AUC



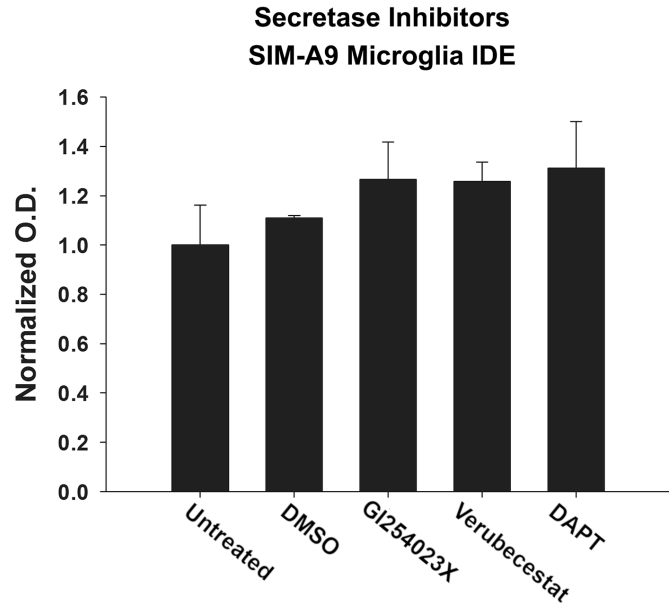
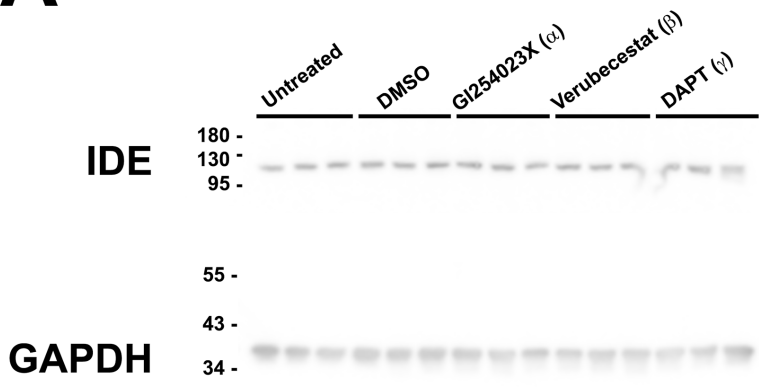
Fed Blood Glucose



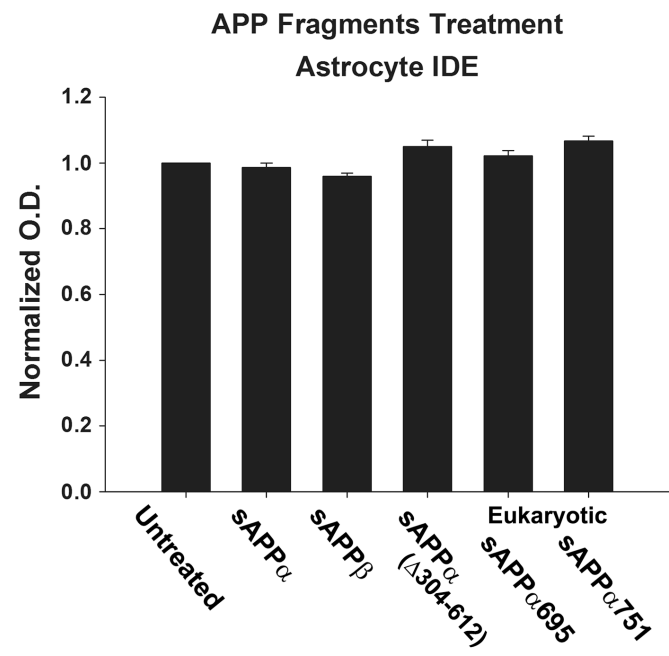
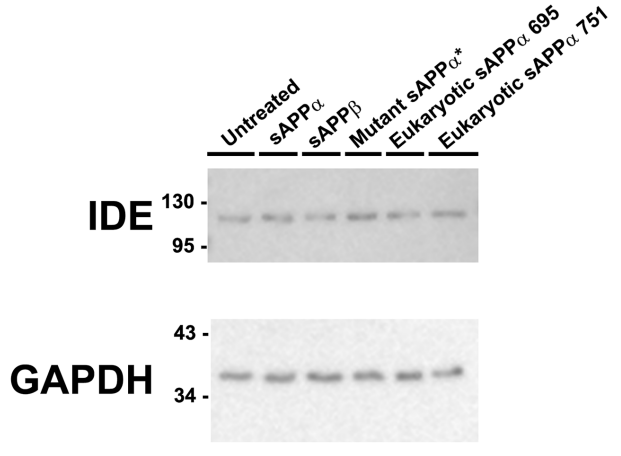
Fasting Blood Glucose



A SIM-A9 Microglia - Secretase Inhibitors



B APP-/- Astrocyte Cultures



C APP-/- Astrocyte Cultures

